LATVIAN JOURNAL of PHYSICS and TECHNICAL SCIENCES

ISSN 0868 - 8257

(Vol. 55)

2018

SATURS

Latvijas Universitātes Cietvielu fizikas institūta (LU CFI) rīkotās starptautiskās konferences "FUNKCIONĀLIE MATERIĀLI UN NANOTEHNOLOĢIJAS FM&NT-2018" (Rīga, 2018. gada 2. līdz 5. oktobrim) **materiāli**

CONTENTS

Materials of the International Scientific Conference
"FUNCTIONAL MATERIALS & NANOTECHNOLOGIES"-2018
(Institute of Solid State Physics, University of Latvia, Riga, 2–5 October 2018)

СОДЕРЖАНИЕ

Материалы международной научной конференции
«ФУНКЦИОНАЛЬНЫЕ МАТЕРИАЛЫ И НАНОТЕХНОЛОГИИ –2018»
(Институт физики твердого тела Латвийского университета,
Рига, 2–5 октября 2018 г.)

LATVIAN JOURNAL of PHYSICS and TECHNICAL SCIENCES

LATVIJAS FIZIKAS un TEHNISKO ZINĀTŅU ŽURNĀLS

ЛАТВИЙСКИЙ ФИЗИКО-ТЕХНИЧЕСКИЙ ЖУРНАЛ

Published six times a year since February 1964
Iznāk sešas reizes gadā kopš 1964. gada februāra
Выходит шесть раз в год с февраля 1964 года

6 (Vol. 55) • 2018

RĪGA

INDEKSĒTS (PUBLICĒTS) | INDEXED (PUBLISHED) IN

www.scopus.com
www.sciendo.com
EBSCO (Academic Search Complete, www.epnet.com), INSPEC (www.iee.org.com).
VINITI (www.viniti.ru), Begell House Inc/ (EDC, www.edata-center.com).

Izdevēji: Fizikālās enerģētikas institūts, LU Cietvielu fizikas institūts
Reģistrācijas apliecība Nr. 000700221
Redakcija: Krīvu iela 11, Rīga, LV-1006
Tel. 67551732
e-pasts: ezerniec@edi.lv
Interneta adrese: www.fei-web.lv

sciendo

LATVIAN JOURNAL OF PHYSICS
AND TECHNICAL SCIENCES
2018, N 6

FUNCTIONAL MATERIALS & NANOTECHNOLOGIES

LATVIJAS UNIVERSITĀTES CIETVIELU FIZIKAS INSTITŪTS
INSTITUTE OF SOLID STATE PHYSICS UNIVERSITY OF LATVIA
1978 2018

Conference
"Functional Materials and Nanotechnologies – 2018"

In 2018, Latvia celebrates the 100th anniversary of the declaration of Latvian independence. Our neighbours – Estonia and Lithuania – are celebrating their centenaries of statehood as well. With festivities at home and all over the world, the Baltic countries will present the best they can offer in culture, lifestyle, and innovation.

The FM&NT-2018 conference on advanced materials and nanotechnologies falls under materials scientists' contribution to the national anniversaries of the Baltic countries this year.

This conference is a continuation of annual meetings, first of which was organised in 2006 by the Institute of Solid State Physics, University of Latvia (ISSP UL) in Riga. Since 2013, the FM&NT conference has turned over a new page – becoming a joint conference of all three Baltic countries. Now it is organised on a regular basis by the ISSP of the University of Latvia, University of Tartu, and Vilnius University. The FM&NT is also a tribute to the 40th anniversary of the ISSP UL and centenary celebration of the University of Latvia in 2019.

The aim of the conference has been to bring together materials scientists, physicists, chemists, research staff, engineers, as well as experts in a wide range of the most demanding application areas, and students from universities, research institutes and related industrial companies. The conference topics include:

Optical materials;

Nanocomposites and ceramics;

Thin films and coatings;

Energy harvesting and storage;

Electronic and photonic devices, etc.

Six plenary talks, 19 invited talks, 37 oral presentations and over 130 posters of high scientific quality have been presented at the conference.

Anatolijs Šarakovskis,
Chairman of the Programme Committee of FM&NT-2018

sciendo

LATVIAN JOURNAL OF PHYSICS
AND TECHNICAL SCIENCES
2018, N 6

DOI: 10.2478/lpts-2018-0038

COMPARISON OF LUMINESCENCE IN $LiGaO_2$, Al_2O_3-Ga AND Al_2O_3-Li CRYSTALS

L. Trinkler[1], A.Trukhin[1], Mitch M.C. Chou[2]

[1]Institute of Solid State Physics, University of Latvia,
8 Kengaraga Str., LV-1063 Riga, LATVIA
[2]Center of Crystal Research, National Sun Yat-sen University,
Kaohsiung, TAIWAN
trinkler@latnet.lv

We have studied luminescence of $LiGaO_2$, Al_2O_3-Ga and Al_2O_3-Li crystals in order to reveal the nature of luminescence centres and mechanisms in these crystals. In Al_2O_3-Ga presence of Ga impurities determines occurrence of the 280 nm emission band, which demonstrates intra-centre character in photoluminescence and recombination character under X-ray irradiation. In Al_2O_3-Li crystal lithium induced luminescence is presented with the 326 nm band, which has a recombination character. Basing on spectral similarity of the main luminescence bands in pure $LiGaO_2$ crystal with the dopant-induced emission bands in Al_2O_3, and on peculiarities of the X-ray induced thermoluminescence, the adjustment of the previous luminescence interpretation is done. It is proposed that the donor-acceptor pairs with random separation distribution responsible for the 280 nm emission are represented with gallium Ga (plus an electron) and O (plus a hole) pairs, while the donor-acceptor pairs, producing the 330 nm emission band contain a lithium ion, presumably in the interstitial position Li_i^0, and a neighbouring oxygen ion with a caught hole.

Keywords: *alumina, donor-acceptor pairs, exciton, lithium metagallate, luminescence*

1. INTRODUCTION

Recently we have studied luminescence properties of the wide band gap crystal lithium metagallate $LiGaO_2$ (LGO) (optical gap around 6 eV [1]) grown by authors of [2] and found out that the main emission bands are located at 280 and 330 nm, (4.43 and 3.76 eV), correspondingly, see Fig.1. [3]. The 280 nm band is excited only in the range of intrinsic absorption including the exciton-like sharp band at ~6 eV (206 nm), while the 340 nm band is also excited within optical transparency range peaking at 220 nm. The 280 nm band was assigned to recombination luminescence of randomly separated donor-acceptor pairs (DAPs); the 340 nm band also

demonstrated recombination character [3]. However, the components of the donor-acceptor pairs remained unknown. In the given paper, we present the results of the investigation of alumina Al_2O_3 (AO) doped with impurities Ga and Li, constituting the lattice of LGO, in order to find peculiarities in luminescence of these materials, which could shed light on luminescence mechanisms and DAP composition in LGO. On the other hand, investigation of Al_2O_3 with different dopants could enlarge the application range of this prospective material, mainly known for its outstanding dosimetric properties, when doped with carbon, causing the oxygen deficiency.

There are some studies of luminescence properties of Ga doped AO done before. Cathodoluminescence [4] studies showed presence of the emission band at about 4.5 eV, which was ascribed to Ga luminescence centre. The same emission band was found in the photoluminescence process, under UV light excitation above 6 eV [4]. The same emission band appeared in thermally stimulated luminescence (TL) after x-ray irradiation [4]. TL peaks were observed at ~200 K and ~ 580 K. According to our knowledge, there is no much information on luminescence properties of another object of investigation – AO doped with lithium.

In the given paper, we present luminescence parameters of LGO, AO-Ga and AO-Li obtained under pulsed and continuous photoexcitation as well as X-rays at different temperatures. Additionally X-rays induced TL processes were studied in these materials.

2. EXPERIMENTAL STUDY

The studied nominally pure LGO crystal sample was grown by Czochralski method [2]. The studied AO-Ga crystals were grown by the Verneil method from α-Al_2O_3 powders containing 5 wt% of Ga and were the same as in [4]. Crystal AO–Li was obtained by adding 2 % Li_2O to powders.

Experimental equipment contains different light sources used for luminescence excitation: ArF laser (193 nm) and KrF laser (248 nm), model PSX-100, made by Neweks, Estonia, with pulse energy of about 5 mJ and duration of 5 ns and a deuterium lamp 30 W combined with 0.5 m Seya-Namioka vacuum monochromator. X-ray irradiation was performed by an x-ray tube with tungsten anode operating at 40 kV and 20 mA. A refrigerator with a special sample holder was used allowing cooling down to 10 K and heating up to 750 K.

3. RESULTS

3.1. Photoluminescence and TL of LGO

The newly obtained results on LGO refer to the X-ray induced processes, the main attention being paid to the 280 nm band. It was found that the 280 nm emission band was present in the X ray-induced luminescence (XL) (Fig. 2, curve 1) and in the XL afterglow when the irradiation was ceased (Fig. 2, curve 2). Besides, at temperatures below 80 K this band was also observed in X-ray induced TL emission (Fig. 2, curves 3 and 4), at higher temperatures this band disappeared from the TL emission spectrum (Fig. 2, curve 5). Such behaviour was also demonstrated by the

TL glow curve (Fig. 2, insert) obtained by selecting 280 nm emission. The presence of the 280 nm band in XL afterglow and TL emission spectrum gave an additional argument for the recombination nature of this luminescence band.

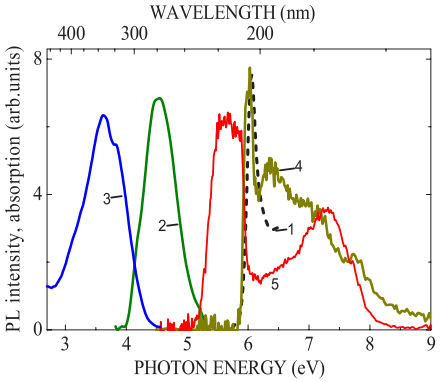

Fig. 1. LGO crystal optical absorption at RT (1) [1,3], PL at laser excitation 193 nm (2) and 248 nm (3); PLE of 280 nm emission (4) and 330 nm emission (5).

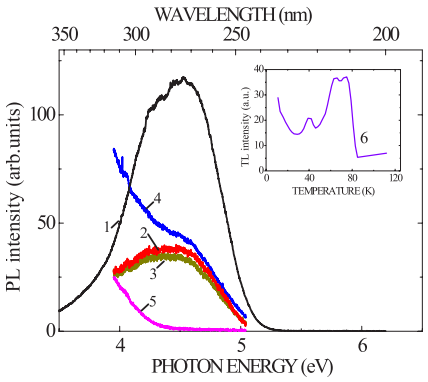

Fig. 2. LGO: XL spectrum at 10 K (1); XL afterglow at 10 K (2); TL emission at 35–45 K (3); 55–75 K (4); 85 K (5). Insert – TL curve (6) selecting luminescence with the 280 nm optical filter.

3.2. Photoluminescence of Al_2O_3-Ga

The main spectral parameters of gallium doped alumina crystal are presented in Fig. 3. Apart from the sharp line in the red part of spectra tentatively assigned to Cr and/or Ti impurities and a blue luminescence bands, both typical for all samples of alumina crystal (not shown in the figures), there is a unique emission band characteristic only of AO-Ga at 280 nm (~4.5 eV) (Fig. 3, curve 1). The corresponding photoluminescence excitation (PLE) spectrum is presented as well (Fig. 3, curve 2) together with the optical absorption spectrum (Fig. 3, curve 3). Excitation band for luminescence at 280 nm starts at around 210 nm (6 eV) with a small band; the main excitation band is situated at 175 nm (7.2 eV).

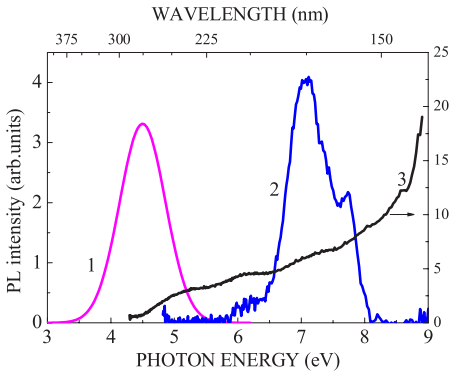

Fig. 3. Photoluminescence spectrum (1) of AO-Ga crystal excited with ArF laser (193 nm; 6,4 eV) and excitation spectrum of the 280 nm band (2) at 60 K. Optical absorption spectrum (3) presented as well.

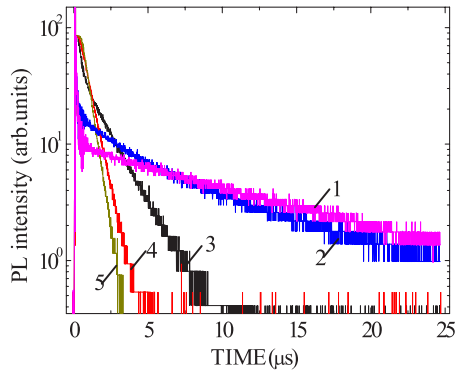

Fig. 4. PL at 280 nm (4.4 eV) decay kinetics of AO-Ga crystal excited with pulses of ArF laser at different temperatures: 60 K (1); 80 K (2); 210 K (3); 261 K (4); 270 K (5).

The 280 nm band in AO-Ga is the main object of interest, because by its spectral properties it resembles the 280 nm band in LGO. The decay kinetics curves under excitation with pulses of ArF laser (193 nm or 6.4 eV) have two components: the fast in the ns range and the slow in the μs range. Thermal evolution of the microsecond component is presented in Fig. 4. It is exponential in all thermal range. Decay time becomes faster with an increase of temperature. The 280 nm emission band of AO-Ga does not appear in afterglow when the ArF laser excitation is switched off. These features of the AO-Ga emission speak in favour of intra-center rather than recombination origin of the luminescence process. According to [4], the 280 nm band is assigned to Ga ion substituting for Al in AO-Ga.

Measuring the time-resolved spectra at 10 K (Fig. 5), we have also found a fast decay component, previously observed under cathode-excitation [4]. The fast component spectrum has a maximum at higher photon energies – 250 nm (4.9 eV) than that for the slow component. We ascribe presence of two emission subbands in the time-resolved spectra to the singlet-triplet splitting and therefore the slow component is ascribed to the triplet-singlet transitions, while the fast component – to the singlet-singlet transitions. In Fig. 6, the time resolved temperature dependence of intensity is compared with that of time constant, both obtained from the same kinetics curves. The thermal dependence of intensity is retarded with respect to the time constant dependence. That can be explained with an increase of transition probability along with an increase of the temperature. It is seen that thermal quenching for the fast luminescence at 250 nm takes place at 80 K. There is good correspondence between dependences of intensity and time constant.

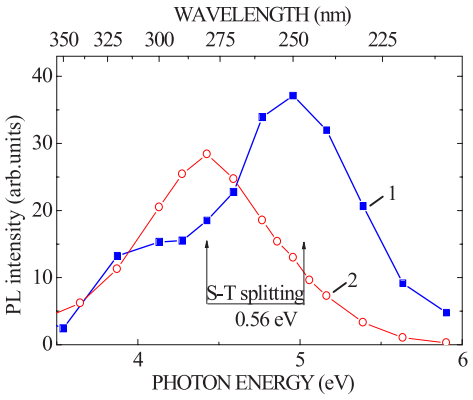

Fig. 5. Time resolved PL spectra of AO-Ga crystal for ns (1) and μs (2) components of decay excited with pulses of ArF laser at 10 K.

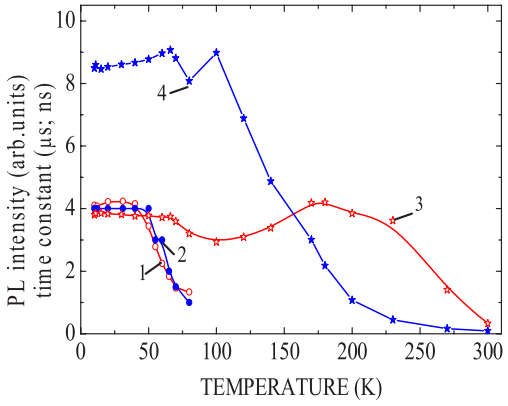

Fig. 6. Time resolved PL intensity and time constant temperature dependences AO-Ga excited with pulses ArF laser. Integral of fast (ns) decay (1); fast time constant (ns) (2); integral of slow (μs) decay (3); slow time constant (μs) (4).

3.3. Photoluminescence of Al_2O_3-Li

The AO-Li sample contains several PL bands. We will not discuss here those bands in the red and blue part of the luminescence spectrum, which are observed in all Al_2O_3 samples without intentional doping.

Spectral parameters of AO-Li luminescence related to Li are presented in Fig. 7. This sample has a band at 326 nm (~3.8 eV) excited with KrF laser (248 nm or 5 eV). Its PLE spectrum measured with use of the 340 nm interference filter (with FWFM 25 nm) shows a number of bands. Decay kinetics curves of the 340 nm luminescence are non-exponential and become faster with an increase of temperature (see Fig. 8).

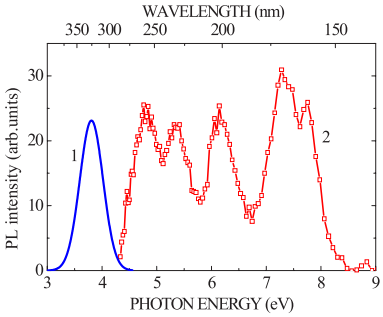

Fig. 7. PL excited at 248 nm (1) and PLE spectra of 330 nm emission of AO-Li (2) at 60 K.

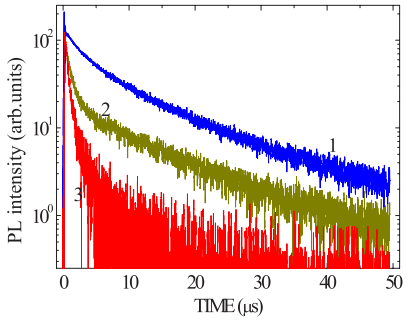

Fig. 8. Decay kinetics of the 320 nm emission band of AO-Li excited with ArF laser at 60 K (1); 80 K (2); 293 K (3).

3.4. Recombination Luminescence of Al_2O_3-Ga and Al_2O_3-Li

After ArF laser irradiation we have observed the TL process only in AO-Li crystal (not shown graphically). In AO-Ga TL has not been observed in similar conditions. The x-ray irradiation causes the TL process in both types of crystals. In Fig. 9 TL emission spectra are shown and compared with those of XL spectra. Under X-rays the doped AO samples in XL and TL emission demonstrate the same bands as in PL spectrum.

In AO-Ga the short wavelength band shifts to longer wavelengths from 280 nm to 300 nm with temperature rise. Another point is that AO-Li luminescence spectrum practically is not measurable in TL. Its XL intensity is also rather low, and what is interesting, higher at RT than at 80 K (see Fig. 9, curves 4 and 5). Figure 10 presents TL curves after x-ray irradiation at 80 K and XL growth and afterglow kinetics (inserts). The AO-Li glow curve contains one peak at 260 K. TL of AO-Ga sample contains the same peak, however, more intense, and also peaks at ~100 K and at 460 K.

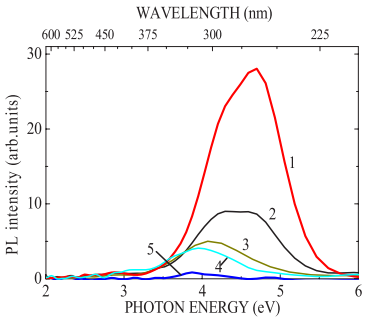

Fig. 9. AO-Ga: XL at 80 K (1); TL spectrum at 180 K (2); TL spectrum at 220 K (3); AO-Li: XL spectrum at 293 K (4); XL spectrum at 80 K (5).

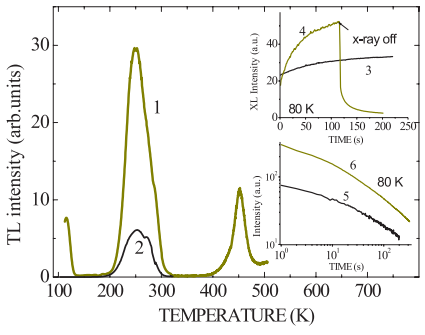

Fig. 10. TL curves of AO-Ga (1) and AO-Li (2) after X-ray irradiation at 80 K. Inserts – XL growth for AO-Li (3) and AO-Ga (4) and XL afterglow for AO-Li (5) and AO-Ga (6).

3. DISCUSSION

In this study, in order to determine the nature of the main PL emission bands of LGO located at 280 and 330 nm (4.43 eV and 3.75 eV), we have investigated luminescence of another wide band material – Al_2O_3 (AO) crystals doped with Li and Ga. In LGO Ga and Li ions belong to the host lattice cations, whereas in AO they are defects – impurity ions. First let us discuss the luminescence of the AO crystals doped with Ga and Li ions.

3.1. Al_2O_3-Ga

We have shown that in AO-Ga presence of Ga impurity determines appearance of the 280 nm (4.43 eV) emission band, with excitation in the 170–210 nm (5.9–7.3 eV) range. Under UV laser irradiation its decay kinetics has two components – in ns and μs range, the latter being exponential. This emission band is not observed in PL afterglow and TL emission. These facts speak in favour of the intra-centre character of the Ga-related luminescence when excited in its own excitation band. The time resolved spectra of this sample allowed distinguishing of the 250 nm band with time constant ~4 ns and the 280 nm band with time constant about 15 μs and assignment of these bands to singlet-singlet and triplet-singlet transitions. The determined value of singlet-triplet splitting is about 0.56 eV, Fig.7. Here we note that in the pure Al_2O_3 luminescence of a self-trapped exciton with 0.25 eV singlet-triplet splitting was detected [5].

Under X-ray excitation the 280 nm emission of AO-Ga is observed in XL afterglow and TL emission, together with XL growth and decay characteristics it definitely confirms the recombination character of the luminescence. The TL curve contains a peak at 260 K, which is characteristic of AO crystal not dependent on dopants [6] and ascribed to an electron trap. The presence of the 260 K curve in the 280 nm TL emission means that there is a hole located on the Ga-related luminescence centre, which recombines radiatively with the released electron.

Summarising the experimental results, we can propose a model of the 280 nm luminescence centre in AO-Ga as a combination of gallium impurity ion and a neighbouring oxygen ion Ga-O. It produces the inter-centre luminescence under UV irradiation; whereas under X-rays it catches a hole, which recombines with an electron resulting in recombination luminescence.

3.2. Al_2O_3-Li

Evidently, presence of Li impurity in AO crystal is responsible for occurrence of the 326 nm emission band, excited in the spectral region below 4.5 eV (150–270 nm). Contrary to the UV-induced PL of Ga-related centre the Li-related PL emission cannot be ascribed solely to the inter-centre process, because its decay curves are not exponential in the range of 50 μs. Both UV and X-ray irradiation produces TL and afterglow with presence of the 326 nm band in this material. These facts characterise the recombination character of the 326 nm emission in AO-Li. Similarly to the Ga case, presence of the 260 K peak in the TL of AO-Li, ascribed to depletion of

electron traps, implies that Li-related luminescence centre contains a hole. In some aspects (spectral position and decay kinetics), this luminescence reminds that from a complex centre in alkali-doped silica glass, containing ions of aluminium, alkali and oxygen [7]. Besides, luminescence of AO-Li is similar to silica glass doped with alkali ions [8]. We propose that in AO-Li, a complex hole defect containing Li and oxygen ions is responsible for the 326 nm emission of recombination character.

Al_2O_3 doped with Ga and Li ions produce TL response located in suitable for registration spectral and thermal region; however, its intensity, at least with the used dopant concentrations, is too low to be used for dosimetry needs.

3.3. $LiGaO_2$

The main luminescence bands of LGO at 280 (4.43 eV) and 330 nm (Fig. 1) have already been studied in [3]. The 280 nm band is excited in the spectral range, corresponding to the exciton states (a sharp feature at 6 eV) and band-to-band transitions. Based on the luminescence features such as superposition of exponents in the luminescence decay pulses (similar to luminescence properties in Ga_2O_3 crystal [9]), blue shift of the emission band and decrease of thermal quenching rate with an increase of the excitation light intensity, it has been proven that this emission results mainly from tunnel recombination of donor-acceptor pairs (DAP) with the random distribution of separation distance [3]. In the present study, we have got the additional confirmation of the recombination character of this emission – the 280 nm emission band has been observed in X-ray induced processes: XL afterglow and TL emission spectra at temperatures below 80 K. Presence of the DAP recombination with participation of the crystal host components means that the irradiation-produced charge carriers – electrons and holes – are self-trapped on the regular lattice sites. Comparing luminescence spectra of the studied crystals, one can find that the 280 nm emission band of LGO is similar to Ga-related emission band in AO-Ga: spectral position of emission and excitation coincides. From this fact, we can propose that the 280 nm band of LGO also results from a luminescence centres, containing Ga ion. The most probable candidates for DAP are Ga and O ions, with the self-trapped charge carriers – electrons and holes, correspondingly, producing Ga(e) and O(h) pairs with different separation distance. The closest pairs are identical to self-trapped excitons.

The 330 nm emission band in LGO was ascribed to recombination luminescence of geminate DAPs [3]. This band was observed in PL and UV-induced TL emission, dependence on excitation intensity was not found. It is comparable with the 326 nm Li-related emission band in AO-Li, the excitation range below 5 eV is also similar in these 2 crystals. Position of the excitation band in LGO below the conduction band implies that the luminescence centre is a defect of the crystalline lattice, while similarity with Li-related emission in AO speaks in favour of Li ion involvement. We propose that this could be interstitial lithium Li_i, perhaps with a lithium vacancy v_{Li} nearby. After irradiation an interstitial will catch an electron and convert into Li_i^0, while a hole will be caught by an oxygen ion converting it to O^0. Radiative recombination of such DAP containing Li_i produces the 330 nm emission band.

4. CONCLUSIONS

In the present paper, we have studied luminescence properties of Al_2O_3-Ga and Al_2O_3-Li and used the experimental results for adjustment of $LiGaO_2$ luminescence origin.

In Al_2O_3-Ga, the presence of Ga impurity is responsible for the occurrence of the 280 nm luminescence band, excited in 170-310 nm range. We propose a model for the luminescence centre as combination of gallium ion substituting for aluminum ion and a neighbouring oxygen ion: Ga-O. Under UV excitation it produces the inter-centre PL, while under X-rays it catches a hole, which radiatively recombines with an electron.

In Al_2O_3-Li lithium induced luminescence is presented with a 326 nm band, excited below 270 nm. We propose that in AO-Li, a complex defect containing Li and oxygen ions is responsible for the 326 nm emission of recombination character.

Spectral similarity is found between emission bands of $LiGaO_2$ and Al_2O_3 doped with Ga and Li ions, constituting lattice elements of LGO. Together with the newly found occurrence of the 280 nm in the X-ray induced luminescence afterglow and TL it allows for interpretation of this emission band in LGO as tunnel recombination of Ga (plus an electron) and O (plus a hole) pairs with random separation distance. Generation of these DAPs implies self-trapping of charge carriers; the closest pairs are identical to self-trapped excitons. The 330 nm band of LGO originates from geminate DAPs, involving lithium, presumably in the interstitial position Li_i^0, and neighbouring oxygen with a hole.

TL measurements of Al_2O_3-Ga and Al_2O_3-Li show that these materials, at least with the used dopant concentration, are not suitable for dosimetry needs due to the low TL response to UV and ionizing radiation.

ACKNOWLEDGEMENTS

The present research has partly been sponsored by the Latvian Council of Science, Grant No. lzp-2018/1-0361

REFERENCES

1. Tumėnas, S., Mackonis, P., Nedzinskas, R., Trinkler, L., Berzina, B., Korsaks, V., … Chou, M. M. C. (2017). Optical properties of lithium gallium oxide. *Applied Surface Science*, *421*, 837–842.
2. Chen, C., Li, C.-A., Yu, S.-H., & Chou, M.M.C. (2014). Growth and characterization of β-$LiGaO_2$ single crystal. *J. Cryst. Growth, 402,* 325–329.
3. Trinkler, L., Trukhin, A., Berzina, B., Korsaks, V., Ščajev, P., Nedzinskas, R., … Li, C.-A. (2017). Luminescence properties of $LiGaO_2$ crystal. *Optical Materials*, *69*, 449–459.
4. Jansons, J., Kulis, A., Rachko, Z., Springis, M., Tale, I., & Valbis, J. (1983). Luminescence of Ga-Doped α-Al_2O_3 Crystals. Phys. *Stat. Sol., (b) 120.* 511–518.
5. Namozov, B., Fominich, M., Myurk, V., & Zakharchenya, R. (1998). *Phys. Solid State 40*, 837–838.

6. Springis, M., Kulis, P., & Tale, I. (1995). Point defects related to 260 K thermostimulated luminescence in α- Al_2O_3. *Radiation Effects and Defects in Solids, 134,* 481–483.
7. Trukhin, A.N., Jansons, J.L., & Truhins K. (2004). Luminescence of silica glass containing aluminum oxide. *Journal of Non-Crystalline Solids, 347*(1–3), 80–86.
8. Trukhin, A., & Rudenko, V. (1987). Spectral-kinetic investigations of luminescence centers – Non-bridging oxygen-one valence ion. *Soviet Glass Physics and Chemistry 13*, 236–241. (in Russian)
9. Binet, L., & Gourier, D. (1998). Origin of the blue luminescence of β-Ga_2O_3. *J. Phys. Chem Solids, 59,* 1241–1249.

SALĪDZINOŠS LUMINISCENCES PĒTĪJUMS $LiGaO_2$, Al_2O_3-Ga UN Al_2O_3-Li KRISTĀLOS

L.Trinklere, A. Truhins, M. Čou

K o p s a v i l k u m s

$LiGaO_2$, Al_2O_3-Ga and Al_2O_3-Li kristālu luminiscence tika pētīta, lai noskaidrotu luminiscences mehānismus un centrus šajos materiālos. Kristālā Al_2O_3-Ga pateicoties Ga piemaisījuma klātbūtnei parādās luminiscences josla 280 nm, kurai piemīt iekšcentra raksturs fotoluminiscences gadījumā un rekombinācijas raksturs rentgenluminiscencē. Kristālā Al_2O_3-Li luminiscences josla 326 nm ir saistīta ar litija piemaisījumu, tai ir noteikts rekombinācijas raksturs. Tiek piedāvāta precizēta interpretācija litija gallija oksīda luminiscencei, ņemot vērā $LiGaO_2$ galveno luminiscences joslu līdzību ar piemaisījumu izraisītām luminiscences joslām Al_2O_3 kristālos. Šajā materiālā 280 nm luminiscences josla rodas pateicoties donoru-akceptoru pāru rekombinācijai, kur donori un akceptori ir Ga ar saķertu elektronu un O ar saķertu caurumu, bet 330 nm luminiscences josla atbilst tādu donoru-akceptoru pāru rekombinācijai, kur piedalās litija jons Li_i^0 un blakusesošais skābeklis ar saķertu caurumu.

20.11.2018.

sciendo

LATVIAN JOURNAL OF PHYSICS
AND TECHNICAL SCIENCES
2018, N 6

DOI: 10.2478/lpts-2018-0039

INFLUENCE OF PRESSURE AND TEMPERATURE ON X-RAY INDUCED PHOTOREDUCTION OF NANOCRYSTALLINE CuO

A. Kuzmin [1], A. Anspoks [1], L. Nataf [2], F. Baudelet [2], T. Irifune [3]

[1] Institute of Solid State Physics, University of Latvia,
8 Kengaraga Str., Riga, LV-1063, LATVIA
E-mail: a.kuzmin@cfi.lu.lv
[2] Synchrotron SOLEIL, l'Orme des Merisiers, Saint-Aubin,
BP 48, 91192 Gif-sur-Yvette, FRANCE
[3] Geodynamics Research Center, Ehime University,
2-5 Bunkyo-cho, Matsuyama, Ehime 790-8577, JAPAN

X-ray absorption spectroscopy at the Cu K-edge is used to study X-ray induced photoreduction of copper oxide to metallic copper. Although no photoreduction has been observed in microcrystalline copper oxide, we have found that the photoreduction kinetics of nanocrystalline CuO depends on the crystallite size, temperature and pressure. The rate of photoreduction increases for smaller nanoparticles but decreases at low temperature and higher pressure.

Keywords*: copper oxide, high-pressure, nanocrystalline, radiolysis, x-ray absorption spectroscopy*

1. INTRODUCTION

Nanocrystalline copper(II) oxide (CuO) attracts much attention due to a wide range of possible applications, including gas sensors, catalysis, batteries, supercapacitors, field emission displays, nanoenergetic materials, photodetectors and solar cells [1]. Better understanding and optimization of device operation requires monitoring of the oxide structure-functional property relationship under *in situ* and *in operando* conditions. Nowadays such studies widely involve experiments utilising high-intensity synchrotron X-ray radiation [2]–[5].

It is known that in some cases the intense incident X-ray beam may alter the conditions of the experiment and lead to changes in chemical structure and properties of a sample. In particular, a reduction of metal ions, including Cu^{2+}, occurs in aqueous solutions due to radiolysis [6], [7]. Therefore, this effect finds an application for synthesis of metal nanoparticles [6]–[12]. The radiolysis process causes the production of reducing radicals such as hydrated electrons and hydrogen atoms under

X-ray or γ-ray irradiation of a solution [13], [14].

In this study, we use a polychromatic focused synchrotron X-ray radiation to follow kinetics of nanocrystalline CuO photoreduction as a function of crystallite size, temperature and pressure. Note that we deliberately neglected this effect in our recent study of copper oxide at high pressure due to a short time of the experiment [15].

2. EXPERIMENTAL STUDY

Nanocrystalline CuO was prepared by a decomposition of $Cu(OH)_2$ precipitate in air at the two temperatures of 130 °C and 150 °C [16]. The precipitate was produced by the reaction of aqueous solutions of copper nitrate and sodium hydroxide. Commercial polycrystalline CuO powder (Adrich, 99+% purity) was used for comparison.

X-ray powder diffraction patterns (Fig. 1) of CuO samples were measured at room-temperature using the Bruker AXS D2 PHASER Bragg-Brentano θ/θ diffractometer equipped with the LynxEye detector and copper anode (Cu Kα) tube. The samples were rotated during the measurements, and their patterns were collected in the angular range 2θ from 10° to 90° with the step of Δ(2θ)=0.04°. The lattice parameters and crystallite sizes were evaluated from the analysis of diffraction patterns by the Rietveld method [17] using the Profex code [18].

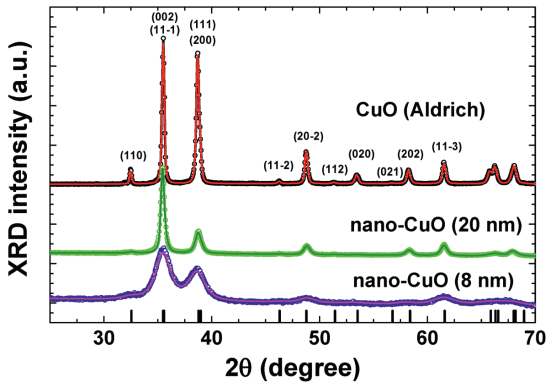

Fig. 1. Powder X-ray diffraction patterns of CuO: open circles – experiments, solid lines – Rietveld refinements. The vertical bars correspond to monoclinic CuO phase (space group C2/c (No. 15)) [19].

Pressure and temperature dependent Cu K-edge X-ray absorption spectroscopy studies of nanocrystalline and microcrystalline CuO samples were performed using the dispersive setup of the ODE beamline at SOLEIL synchrotron [20]. The SOLEIL synchrotron operated in the top-up mode with the energy E=2.75 GeV and current I=450 mA. The X-ray synchrotron radiation, produced by bending magnet, was dispersed and focused by a cooled single-crystal Si(111) monochromator bent in four points. The polychromatic photon flux on the sample was about 109 photons/s/eV in 25×35 μm FWHM. Two mirrors installed before and after the monochromator were used for a harmonic rejection. X-ray absorption spectra were recorded by

a Princeton Instruments PIXIS-400 CCD camera coupled with a scintillator. The sample pressure and temperature were controlled using a membrane-type nano-polycrystaline diamond anvil cell (NDAC) [21], [22] and liquid helium cryostat. The silicon oil (Rhodorsil Oils 47V100) was used as pressure transmitting media. The pressure in the cell was monitored using the position of the R1-line of ruby fluorescence excited by a 473 nm DPSS laser.

3. RESULTS AND DISCUSSION

The results of the Rietveld refinement of the X-ray diffraction patterns (Table 1) suggest that the lattice parameters of nano-sized CuO are close to that of microcrystalline powder. Some evidence of the lattice expansion upon crystallite size reduction is observed; however, the effect is rather small. Note that the unit cell volume expansion was found previously in CuO powders with the average grain size of about 9.5–35.1 nm and explained by an influence of strain or oxygen depletion [23].

Table 1

Lattice Parameters Obtained by Rietveld Refinement

	CuO (Aldrich)	nano-CuO (20 nm)	nano-CuO (8 nm)
a (Å)	4.6861(2)	4.6823(8)	4.710(4)
b (Å)	3.4272(2)	3.4289(8)	3.448(4)
c (Å)	5.1335(2)	5.1390(5)	5.143(3)
b (°)	99.428(2)	99.419(8)	99.10(4)
y(O)	0.433(3)	0.390(5)	0.46(3)
V (Å3)	81.34	81.40	82.47
d (nm)	70(3)	20(2)	8(1)

The effect of temperature on the X-ray induced photoreduction of nano-CuO (8 nm) is shown in Fig. 2 for three temperatures (10, 190 and 260 K) at the pressure P =1–2 GPa. The appearance of metallic copper is well visible at T =260 K as a growing shoulder at 8983 eV and a reducing main peak at 9000 eV. However, the reduction process is not fully completed even after 70 min.

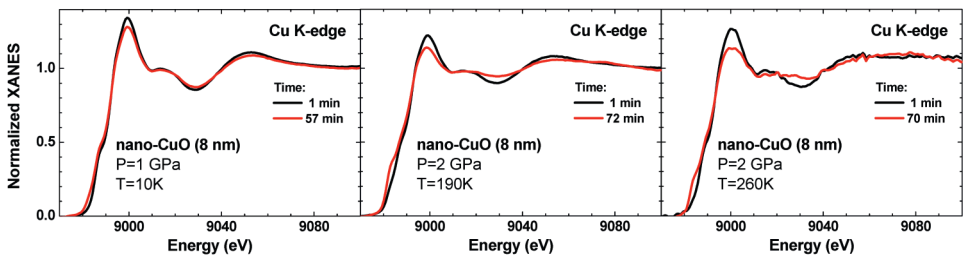

Fig. 2. Temperature-dependent Cu K-edge XANES of nano-CuO (8 nm) at P = 1-2 GPa as a function of experimental time.

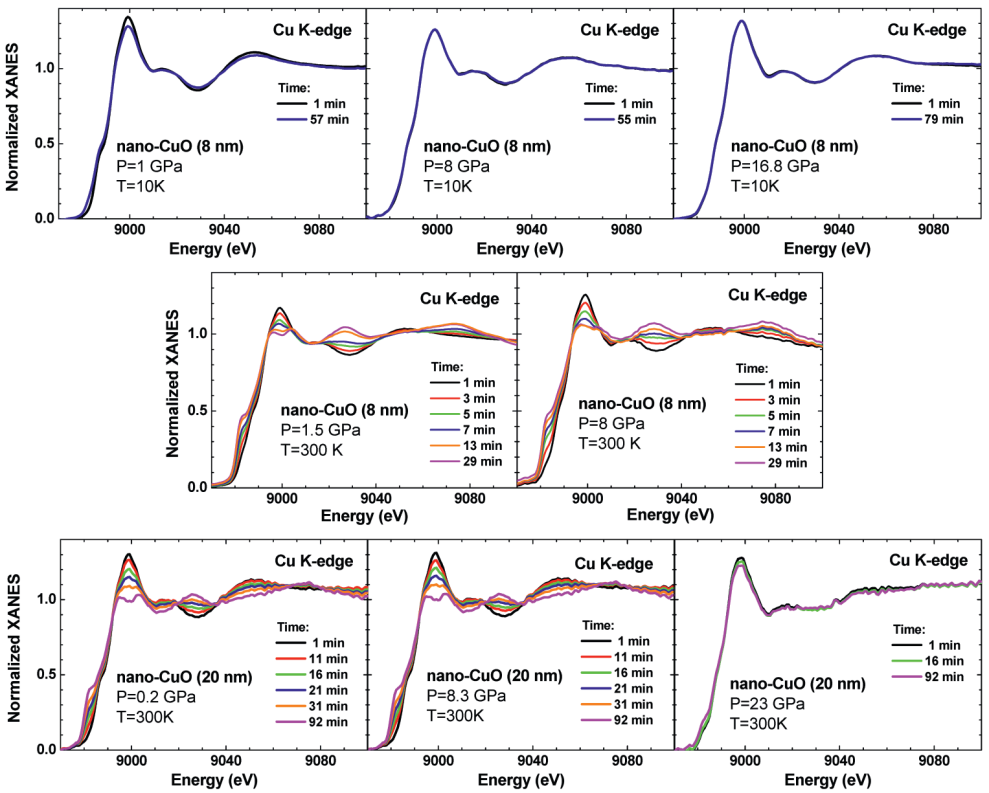

Fig. 3. Pressure-dependent Cu K-edge XANES of nano-CuO (8 and 20 nm) at T =10 and 300 K GPa as a function of experimental time.

A decrease of temperature down to 10 K significantly slows down the photoreduction of the oxide to metallic copper. At low temperature (10 K), the photoreduction of small (8 nm) CuO nanoparticles occurs only at low pressure (P =1 GPa), whereas no effect is visible at 8 and 16.8 GPa (upper panels in Fig. 3). Thus, a retardation of the photoreduction effect due to radiolysis can be achieved by increasing pressure.

At the same time, a complete conversion of nano-CuO (8 nm) to metallic copper occurs for about 0.5 h at 300 K for the pressure below ~8 GPa (middle panels in Fig. 3). Upon increasing crystallite size to 20 nm, the reduction process takes more time (about 1.5 h) at the pressure below ~8.3 GPa (lower panels in Fig. 3). Further increase of pressure up to 23 GPa stabilizes the oxide phase in 20 nm CuO crystallites.

4. CONCLUSIONS

X-ray induced photoreduction of copper oxide placed in a diamond anvil cell has been studied using synchrotron radiation X-ray absorption spectroscopy at the Cu K-edge as a function of crystallite size, temperature and pressure. We have not observed any photoreduction in the case of microcrystalline copper oxide, but it has clearly been detected from the change in X-ray absorption near edge structure of

nanocrystalline CuO. The rate of CuO photoreduction to metallic copper increases with a decrease in nanoparticle size, but slows down with a decrease in temperature or an increase in pressure. These findings are important for all studies dealing with high-flux X-ray beams, in particular, in the case of nanosized CuO catalysts.

ACKNOWLEDGEMENTS

The authors are grateful to Prof. Alain Polian for providing NDAC cell. Parts of the present research have been carried out at the ODE beamline at SOLEIL.

REFERENCES

1. Zhang, Q., Zhang, K., Xu, D., Yang, G., Huang, H., Nie, F., …Yang, S. (2014). CuO nanostructures: Synthesis, characterization, growth mechanisms, fundamental properties, and applications. *Prog. Mater. Sci., 60*, 208–337. DOI: 10.1016/j.pmatsci.2013.09.003
2. Frenkel, A. I., Rodriguez, J. A., & Chen, J. G. (2012). Synchrotron techniques for in situ catalytic studies: Capabilities, challenges, and opportunities. *ACS Catal., 2*, 2269–2280. DOI: 10.1021/cs3004006
3. Volanti, D. P., Felix, A. A., Suman, P. H., Longo, E., Varela, J. A., & Orlandi, M. O. (2015). Monitoring a CuO gas sensor at work: An advanced in situ X-ray absorption spectroscopy study. *Phys. Chem. Chem. Phys.*, *17*, 18761–18767. DOI: 10.1039/C5CP02150B
4. Lin, F., Liu, Y., Yu, X., Cheng, L., Singer, A., Shpyrko, O. G., … Doeff, M. M. (2017). Synchrotron X-ray analytical techniques for studying materials electrochemistry in rechargeable batteries. *Chem. Rev.*, *117*, 13123–13186. DOI: 10.1021/acs.chemrev.7b00007
5. Liguang, W., Jiajun, W., & Pengjian, Z. (2018). Probing battery electrochemistry with in operando synchrotron X-ray imaging Techniques. *Small Methods*, 1700293. DOI: 10.1002/smtd.201700293
6. Joshi, S., Patil, S., Iyer, V., & Mahumuni, S. (1998). Radiation induced synthesis and characterization of copper nanoparticles. *Nanostruct. Mater.*, 10, 1135–1144. DOI: 10.1016/S0965-9773(98)00153-6
7. Yamaguchi, A., Okada, I., Fukuoka, T., Ishihara, M., Sakurai, I., & Utsumi, Y. (2016). One-step synthesis of copper and cupric oxide particles from the liquid phase by X-ray radiolysis using synchrotron radiation. *J. Nanomater*., *2016*, 8584304. DOI: 10.1155/2016/8584304
8. Oyanagi, H., Sun, Z. H., Jiang, Y., Uehara, M., Nakamura, H., Yamashita, K., … Maeda, H. (2012). Small copper clusters studied by X-ray absorption near-edge structure. *J. Appl. Phys.*, *111*, 084315. DOI: 10.1063/1.3700346
9. Jayanetti, S., Mayanovic, R. A., Anderson, A. J., Bassett, W. A., & Chou, I. M. (2001). Analysis of radiation-induced small Cu particle cluster formation in aqueous $CuCl_2$. *J. Chem. Phys.*, *115*, 954–962. DOI: 10.1063/1.1379758
10. Lee, H. J., Je, J. H., Hwu, Y., & Tsai, W. (2003). Synchrotron X-ray induced solution precipitation of nanoparticles. *Nucl. Instrum. Methods Phys. Res. B, 199*, 342–347. DOI: 10.1016/S0168-583X(02)01561-6
11. Oyanagi, H., Orimoto, Y., Hayakawa, K., Hatada, K., Sun, Z., Zhang, L., … Maeda, H. (2014). Nanoclusters synthesized by synchrotron radiolysis in concert with wet chemistry. *Sci. Rep*., *4*, 7199. DOI: 10.1038/srep07199

12. Mukherjee, S., Fauré, M. C., Goldmann, M., & Fontaine, P. (2015). Two step formation of metal aggregates by surface X-ray radiolysis under langmuir monolayers: 2D followed by 3D growth. *Beilstein J. Nanotechnol*., *6*, 2406–2411. DOI: 10.3762/bjnano.6.247
13. Jonah, C. D. (1995). A short history of the radiation chemistry of water. *Radiat. Res*., *144*, 141–147. DOI: 10.2307/3579253
14. Le Caer, S. (2011). Water radiolysis: Influence of oxide surfaces on H_2 production under ionizing radiation. *Water*, *3*, 235–253. DOI: 10.3390/w3010235
15. Kuzmin, A., Anspoks, A., Kalinko, A., Rumjancevs, A., Timoshenko, J., Nataf, L., … Irifune, T. (2016). Effect of pressure and temperature on the local structure and lattice dynamics of copper(II) oxide. *Phys. Procedia*, *85*, 27–35. DOI: 10.1016/j.phpro.2016.11.077
16. Tran, T. H., & Nguyen, V. T. (2014). Copper oxide nanomaterials prepared by solution methods, some properties, and potential applications: A brief review. *Int. Sch. Res. Notices*, *2014*, 856592. DOI: 10.1155/2014/856592
17. Rietveld, H. (1967). Line profiles of neutron powder-diffraction peaks for structure refinement. *Acta Crystallogr.*, *22*, 151–152. DOI: 10.1107/S0365110X67000234
18. Doebelin, N., & Kleeberg, R. (2015). Profex: A graphical user interface for the Rietveld refinement program BGMN. *J. Appl. Crystallogr*., *48*, 1573–1580. DOI: 10.1107/S1600576715014685
19. Yamada, H., Zheng, X. G., Soejima, Y., & Kawaminami, M. (2004). Lattice distortion and magnetolattice coupling in CuO. *Phys. Rev. B*, *69*, 104104. DOI: 10.1103/PhysRevB.69.104104
20. Baudelet, F., Kong, Q., Nataf, L., Cafun, J. D., Congeduti, A., Monza, A., … Itié, J. P. (2011). ODE: A new beam line for high-pressure XAS and XMCD studies at SOLEIL. *High Pressure Res*., *31*, 136–139. DOI: 10.1080/08957959.2010.532794
21. Tetsuo, I., Ayako, K., Shizue, S., Toru, I., & Hitoshi, S. (2003). Materials: Ultrahard polycrystalline diamond from graphite. *Nature*, *421*, 599–600. DOI: 10.1038/421599b
22. Ishimatsu, N., Matsumoto, K., Maruyama, H., Kawamura, N., Mizumaki, M., Sumiya, H., & Irifune, T. (2012). Glitch-free X-ray absorption spectrum under high pressure obtained using nano-polycrystalline diamond anvils. *J. Synchrotron Rad.*, *19*, 768–772. DOI: 10.1107/S0909049512026088
23. Bianchi, A. E., Plivelic, T. S., Punte, G., & Torriani, I. L. (2008). Probing the structure of nanograined CuO powders. *J. Mater. Sci.*, *43*, 3704–3712. DOI: 10.1007/s10853-008-2600-7

SPIEDIENA UN TEMPERATŪRAS IETEKME UZ NANOKRISTĀLISKĀ CuO RENTGENSTIMULĒTO FOTOREDUCĒŠANU

A. Kuzmin, A. Anspoks, L. Nataf, F. Baudelet, T. Irifune

K o p s a v i l k u m s

Rentgenabsorbcijas spektroskopija Cu K-malā tika izmantota, lai pētītu spiediena un temperatūras ietekmi uz vara oksīda (CuO) rentgenstimulēto fotoreducēšanu. Šajā procesā notiek vara oksīda transformācija par metālisko varu. Nanokristāliskā vara oksīda fotoreducēšanas kinētika ir atkarīga no kristalītu izmēriem, temperatūras un spiediena. Fotoreducēšanas ātrums palielinās mazās nanodaliņās, bet samazinās zemā temperatūrā un augstā spiedienā.

13.11.2018.

sciendo

LATVIAN JOURNAL OF PHYSICS
AND TECHNICAL SCIENCES
2018, N 6

DOI: 10.2478/lpts-2018-0040

FIRST-PRINCIPLES CALCULATIONS OF OXYGEN DIFFUSION IN Ti-Al ALLOYS

S. E. Kulkova [1, 2], A. V. Bakulin [1, 2], S. S. Kulkov [1]

[1] National Research Tomsk State University,
36 pr. Lenina, Tomsk 634050, RUSSIA
[2] Institute of Strength Physics and Materials Science of
the Russian Academy of Sciences, Siberian Branch,
2/4 pr. Akademichesky, Tomsk 634055, RUSSIA
e-mail: kulkova@ispms.ru

The projector augmented-wave method within the density functional theory is applied to investigate the oxygen diffusion in the intermetallic Ti-Al alloys. It is shown that the highest oxygen absorption energies in Ti-Al alloys correspond to the octahedral Ti-rich sites but the presence of aluminium in the nearest neighbours leads to a substantial decrease in the oxygen absorption energy in the alloys. The migration barriers for the oxygen diffusion between various interstices in the crystal lattice of the Ti-Al alloys are estimated. The preferred migration paths along *a* and *c* axes and limiting barriers of the oxygen diffusion in the alloys are determined. The dependence of the oxygen diffusion coefficient on Ti-Al alloy composition is discussed.

Keywords: *atomic diffusion, electronic structure, oxygen, Ti-Al alloys*

1. INTRODUCTION

Titanium aluminides are considered as the most promising structural materials for the aerospace and aviation applications due to their relatively low density, high melting point, high specific strength and modulus, good creep resistance, etc. [1], [2]. However, the oxidation resistance of Ti_3Al and TiAl alloys is much lower than the desirable one that limits their application at high temperatures [1]–[5]. Although $TiAl_3$ alloy has the highest oxidation resistance among the Ti-Al alloys, it is a rather brittle material because of its low symmetry structure with few slip systems. It is known that the formation of a dense oxide film with a corundum α-Al_2O_3 structure on the surface of alloys with a low titanium content ensures their high oxidation resistance [6], [7]. However, the chemical activity of aluminium decreases with increasing titanium content that in combination with the thermodynamic characteristics of oxides implies a higher stability of interfaces with TiO and TiO_2 rather than

with Al_2O_3 [8]. The growth of mixed oxide layers on the surface of the Ti_3Al and TiAl alloys is responsible for lower oxidation resistance. The outer layers of the oxide films, which are not in contact with the alloys, undergo cracking and partial spallation [9], [10]. Thus, the development of new high temperature structural materials based on titanium aluminides, the mechanical properties of which will be intermediate between the properties of nickel-based superalloys and high-temperature ceramics, is a challenging problem of modern materials science. Therefore, it is necessary to control the structure and properties of the surface layers of Ti–Al alloys and also the conditions of their oxidation. In this context, it is necessary to understand better the mechanism of surface oxidation of the Ti-Al alloys at the microscopic level. This implies theoretical studies of the interaction of oxygen with a surface and its diffusion from the surface into bulk and also in the bulk Ti-Al alloys in dependence on their composition. In the present research, we discuss the oxygen diffusion properties in the bulk of Ti_3Al, TiAl and $TiAl_3$ alloys.

2. METHOD OF CALCULATION

The calculations of atomic and electronic structure of binary alloys were performed by the projector augmented-wave (PAW) method [11], [12] within the density functional theory (DFT) implemented in the plane wave VASP code [13], [14]. The generalized gradient approximation (GGA-PBE) was used for the exchange-correlation functional [15]. The optimization of crystal structure was carried out whilst the forces at atoms were smaller than 0.01 eV/Å. We used a full relaxation scheme, which included changes in the cell volume and its shape alongside with optimization of the atomic positions. A *k*-point mesh of 7×7×7 obtained according to the Monkhorst–Pack scheme was used for the integration over the Brillouin zone in the TiAl and $TiAl_3$ bulk alloys. In the case of Ti_3Al alloy a Γ-centered *k*-point mesh of 7×7×7 was used. The oxygen absorption energy was calculated as follows:

$$E_{abs} = -\left[E_{\mathrm{O/Ti\text{-}Al}} - E_{\mathrm{Ti\text{-}Al}} - 1/2\, E_{\mathrm{O_2}}\right], \tag{1}$$

where $E_{\mathrm{O/Ti\text{-}Al}}$ and $E_{\mathrm{Ti\text{-}Al}}$ are the total energies of the bulk Ti-Al alloy with and without oxygen, respectively, and $E_{\mathrm{O_2}}$ is the total energy of the oxygen molecule. In order to calculate the oxygen atom migration barriers along possible paths, the Climbing Image Nudged Elastic Band method (CI-NEB) [16] was used. The initial positions of images along an elementary path were found by linear interpolation between the initial and final positions of a diffusing atom. During subsequent simultaneous relaxation of all images, each atom was assumed to be elastically bound to the same atom in the neighbouring images. Such an approach allows determining accurately a minimum energy path and a saddle point with the maximum energy. In this case, the relaxation of atomic positions was only performed. The height of the migration barrier was calculated as the difference in the total energies for system with the diffusing atom in the saddle point and in the initial one.

3. RESULTS AND DISCUSSION

The intermetallic Ti_3Al, TiAl and $TiAl_3$ alloys possess $D0_{19}$, $L1_0$ and $D0_{22}$ structures, respectively, as shown in Fig. 1. The interstitial impurities such as oxygen, hydrogen, etc. prefer to be absorbed in the octahedral (O) or tetrahedral (T) interstices. All considered Ti-Al alloys are characterised by several types of the O- or T-sites having different compositions of Al and Ti atoms in the nearest environment. In case of Ti_3Al alloy, there are two O-sites: O1 at the centre of the octahedron formed by six Ti atoms, and O2 at the centre of the octahedron formed by four Ti atoms and two Al atoms. All tetrahedral sites in this alloy are formed by three Ti and one Al atoms. The latter atom can be located in the base of the tetrahedron (T1) or at its vertex (T2).

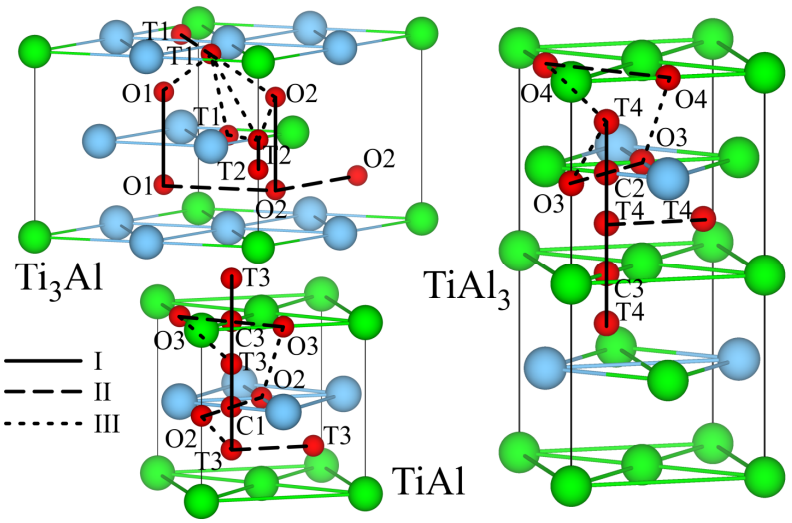

Fig. 1. Atomic structure and oxygen migration paths in the set of Ti-Al alloy. The positions between host atoms in the alloys, i.e., on Ti–Ti, Ti–Al and Al–Al bonds are marked by C1, C2 and C3, respectively.

On the contrary, in $TiAl_3$ alloy the octahedrons are formed primarily by four or five Ti atoms and two or one Al atoms, respectively. The calculated absorption energies of oxygen are given in Table 1. It is seen that the Ti-rich sites are mostly preferable for the oxygen absorption in the bulk alloys that is in agreement with earlier calculations [17], [18]. In a number of works, e.g., [1], [19], it has been concluded that oxygen adsorption takes place on surface titanium atoms and the chemisorption rate decreases when the aluminum concentration in the alloy increases. Moreover, the kinetics for oxidation of Ti-Al alloys, especially at low temperatures, is mainly determined by the growth mechanisms of an oxide scale, i.e., diffusion, rather than surface processes. A slight energy preference of the Al-rich O4-site for the oxygen absorption in $TiAl_3$ alloy is explained by the shift of oxygen towards the Ti atom and, as a result, by the smaller length of the Ti–O bond than in the O3-site, and also by the larger ionic contribution to the mechanism of chemical bond. The lower oxygen absorption energies at the tetrahedral sites correlate with the larger changes in the cell volume; i.e., oxygen can hardly be incorporated in these sites because of smaller

interstice volume. On the whole, the oxygen absorption energies in considered titanium aluminides decrease with an increase of Al atoms in the nearest neighbours and Al content in alloys (Table 1).

Table 1

The Oxygen Absorption Energies in Ti-Al Alloys

Alloys	O1 (6Ti)	O2 (4Ti+2Al)	O3 (2Ti+4Al)	O4 (1Ti+5Al)
Ti_3Al	6.22	4.68	–	–
TiAl	–	4.02	3.07	–
$TiAl_3$	–	–	2.76	2.91
Alloys	T1 (3Ti+1Al)	T2 (3Ti+1Al)	T3 (2Ti+2Al)	T4 (1Ti+3Al)
Ti_3Al	4.58	3.77	–	–
TiAl	–	–	3.17	–
$TiAl_3$	–	–	–	2.85

Let us discuss the diffusion of an oxygen atom along the paths shown in Fig. 1. All migration paths of an oxygen atom can be divided into three groups: (1) paths along the *c* axis, i.e., along [0001] or [001] directions in dependence on symmetry of Ti-Al alloy; (2) paths in the (0001) plane for Ti_3Al or (001) one for TiAl and $TiAl_3$; and (3) paths between sites in different (0001) planes in case of Ti_3Al or (001) ones for other alloys but these sites are not one below another exactly. All calculated migration barriers are summarised in Fig. 2. In Ti_3Al, the highest energy barrier for the oxygen diffusion was obtained between the Ti-rich O1-sites in the [0001] direction. It equals to 3.48 eV that is higher than that for the O2→O2 jump (3.02 eV) in the TiAl alloy. Note that both values for the migration barrier between the preferential O-sites are substantially higher than the value (2.05 eV) obtained for $TiAl_3$ [20]. Thus, despite the differences in the symmetry of the crystal lattices of the Ti–Al alloys, the energy barrier for the oxygen diffusion between the octahedral sites decreases with an increase of the Al content near an oxygen atom. Besides, in Ti_3Al the migration barriers along the O1→O2 and O2→O2 paths in the basal (0001) plane are of ~0.5–0.9 eV lower than those for O1→O1 and O2→O2 along the *c* axis that can indicate the diffusion anisotropy in this alloy.

Although the migration barriers along the O2→O2 path in the [0001] direction and in the basal (0001) plane are lower than for the O1→O1 diffusion in Ti_3Al, it takes higher energy for the O atom to be incorporated into the O2-site, which makes the diffusion between the O2-sites less preferred. In general, the oxygen migration between the T-sites is characterised by a low barrier; however, the path along the [0001] direction does not correspond to translation invariance and can be considered as part of the complex path, e.g., O2→T2→T2→O2. The energy barriers between the T-sites in the plane perpendicular to *c* axis are decreased in the set Ti_3Al–TiAl–$TiAl_3$ (1.87–0.81–0.18 eV). It should be noted that in Ti_3Al the energy barriers of the oxygen diffusion along the paths of the third type (O1→T1, O2→T1, O2→T2, etc., see Fig. 1) are higher than the corresponding barriers in TiAl and $TiAl_3$ alloys. Since the T-sites are less preferable for the O absorption, the reverse diffusion requires lower energy. Finally, it is shown that in TiAl the oxygen diffusion through the Al-layer is almost barrierless, while the migration barrier through the Ti-layer is significantly higher (2.17 eV).

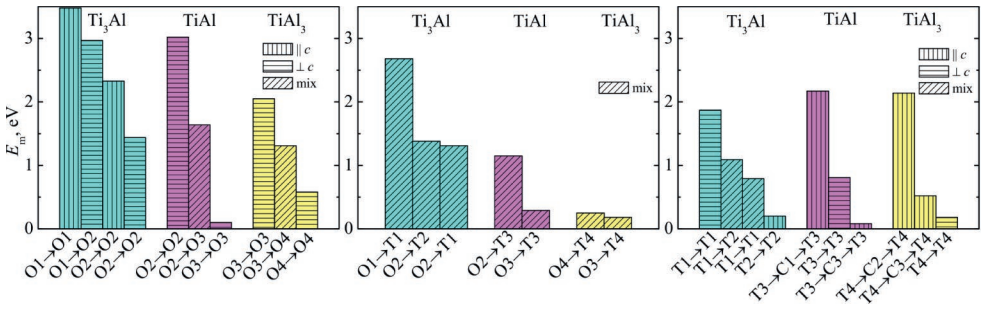

Fig. 2. The calculated migration barrier of oxygen in Ti3Al, TiAl and $TiAl_3$ alloys.

In contrast to [21], in our previous work [22] the diffusion coefficient $D = D_0 \exp(-E_a/k_B T)$, where D_0 – the pre-exponential factor and E_a – the activation energy, was calculated using a specific value of frequency (**v**) for each elementary jump and the corresponding energy barriers along the considered paths. A technique that is an extension of the theory proposed in [23] was used to describe the oxygen diffusion in α-Ti. More details can be found in [22]. As is seen from Fig. 3a, the diffusion coefficient calculated using the energy barriers obtained within the DFT agrees well with the experimental data in [21]. The activation energies calculated from the diffusion coefficient of oxygen in the Ti_3Al alloy along *a* and *c* axes are 1.99 and 1.97 eV, respectively, that agree well with the experimental data (1.94 and 1.92 eV, respectively [21]). The small diffusion anisotropy along two directions also agrees with the conclusion drawn from the experimental data in [21]. However, the oxygen diffusion in TiAl and $TiAl_3$ was not studied despite its importance in understanding the oxidation behaviour and the diffusion barrier properties of the Ti-Al alloys. It is seen from Fig. 3b that the diffusion coefficients of oxygen in both TiAl and $TiAl_3$ alloys are substantially higher than those in Ti_3Al. The difference reaches five-seven order in case of TiAl and $TiAl_3$. With an increase of the Al content, the anisotropy in the diffusion coefficients along *a* and *c* axes and also the oxygen diffusivity in the Al-rich alloys are increased. We remind that the oxidation resistance of the $TiAl_3$ alloy is caused by formation of the dense corundum oxide layers. The fast formation of this thin film prevents the interaction of oxygen with Ti atoms and formation of TiO_2 or mixed oxide scales. The established trends in absorption properties and migration barriers of O in the bulk alloys are valid for the O adsorption on surface and the O migration from the surface into the bulk.

Let us discuss the changes in a local electronic structure of the alloys during the oxygen diffusion along *c* axis. Figure 4 shows the total charge density distribution in the plane perpendicular to *c* axis and passing through the saddle points along different paths in Ti_3Al and $TiAl_3$ alloys. In case of Ti_3Al, the oxygen diffuses between two octahedral sites through the saddle point in triangle (Fig. 4a), whereas in $TiAl_3$ the saddle point is located in bridge position between two atoms (C2 or C3) and the end points are the tetrahedral sites (Fig. 4b). It is seen that in the saddle points the O–Ti bonds have ionic-covalent character, while the O–Al bonds are mainly ionic ones. The change of the charge density distributions has a local character and is accompanied by the shift of the nearest host atoms from O. Since the

covalent radius of Ti atom is larger by 0.14 Å than that of Al one, the presence of Al atoms as the nearest neighbours of oxygen in the saddle point results in an increase of the interstice volume. As a result, it is easier for O atom to be incorporated in this saddle point that leads to lowering of the migration barrier. It is seen in Fig. 4a that the interatomic distance between Ti and O atoms increases by 0.07 Å in presence of Al atom. On the other hand, the appearance of Al near oxygen leads to a decrease of the hybridization contribution that weakens the chemical bonds in saddle point as well. The similar picture can be seen in Fig. 4b.

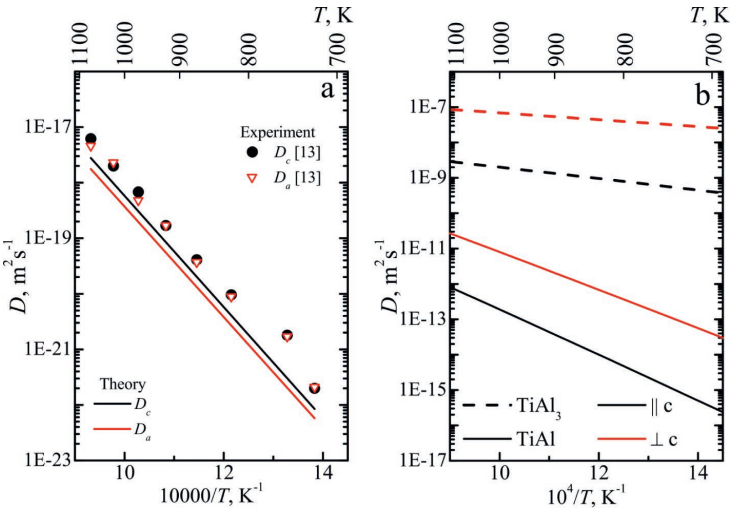

Fig. 3. The calculated diffusion coefficients of oxygen in (a) Ti3Al alloy in comparison with experimental ones and those (b) in TiAl and $TiAl_3$.

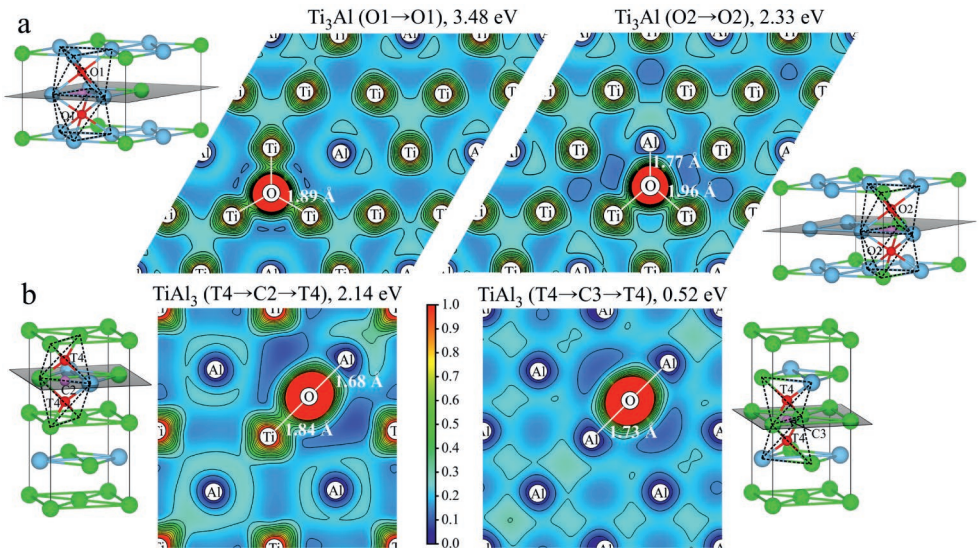

Fig. 4. Total charge density distribution in the plane passing through the oxygen and its nearest host atoms in saddle point for diffusion along c axis in Ti_3Al (a) and $TiAl_3$ (b) alloys. The saddle and end points are shown in corresponding crystal structures.

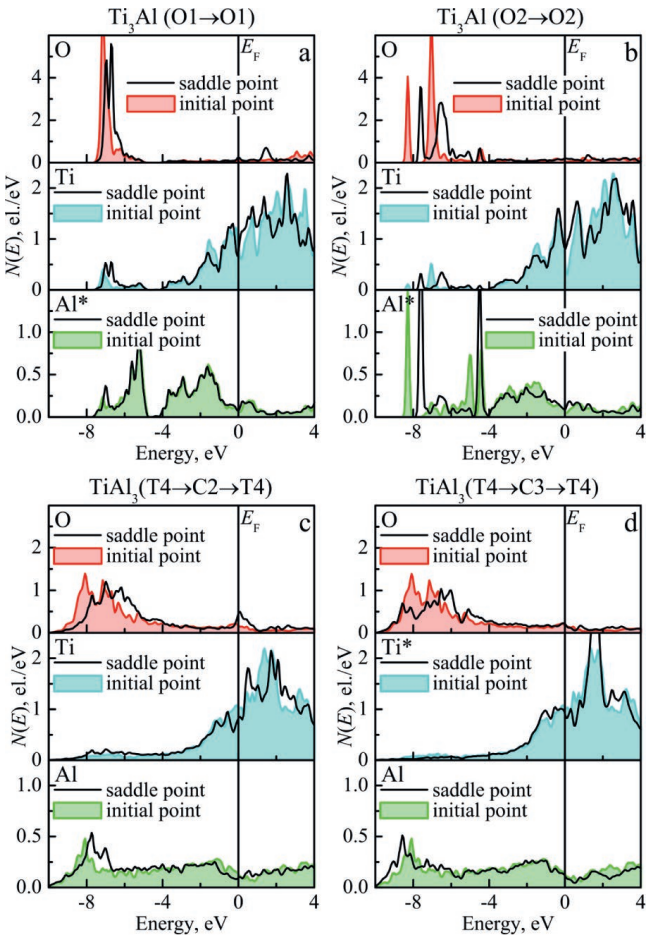

Fig. 5. Local DOS of oxygen and the nearest host atoms in initial and saddle points. The host atoms being the second nearest neighbors to oxygen are marked with symbol *.

The comparison of the local densities of states of O and its nearest neighbour host atoms in the initial and saddle points is given in Fig. 5. It is seen that almost all DOS curves are shifted towards the Fermi level (E_F) in the saddle points. In case of the O diffusion in Ti_3Al (Fig. 5a,b) the density of states at the Fermi level, $N(E_F)$, for Ti and Al atoms increases in the saddle points in comparison with the initial ones. Such changes in the electronic structure of the alloy can be considered as an indicator of structural instability. In the initial points the local DOSs and total ones, being not shown in Fig. 5a,b, have the local minimum in which E_F is located. The opposite effect is observed for the O diffusion between tetrahedral sites in the $TiAl_3$ alloy (Fig. 5c). When O diffuses along the T4→C2→T4 path, there is a decrease of $N(E_F)$ especially in case of Ti atom, while an increase of $N(E_F)$ occurs for O local DOS in the saddle point. However, the total DOS demonstrates the increase of $N(E_F)$ in the C2 saddle point by 3.47 el./eV. We remind that the tetrahedral site is less stable for oxygen in $TiAl_3$ than the octahedral O4-site. For the O diffusion along the T4→C3→T4 path, there are only small changes in the electronic structure of $TiAl_3$ alloy in both initial and saddle points (Fig. 5d) that correlates with the low migration energy.

4. CONCLUSIONS

In the present research, the absorption and diffusion properties of oxygen in the Ti-Al alloys have been calculated by the PAW method within the DFT. It has been shown that the oxygen prefers mainly the Ti-rich octahedral sites in the bulk alloys. The appearance of aluminium in the nearest neighbours of oxygen leads to a decrease of its absorption energy in the set of Ti_3Al–TiAl–$TiAl_3$ alloys. The greater solubility of oxygen in Ti_3Al is connected with existence of the octahedron formed by six Ti atoms. The energy barriers for the oxygen diffusion from preferred absorption sites decrease with an increase of aluminium content in the Ti-Al alloys. *Ab initio* estimations demonstrate that the diffusion coefficient and its anisotropy in the Ti-Al alloys increase also with the Al content. The Ti-rich sites can serve as oxygen traps, which retard the oxygen diffusion and hinder the aluminium oxidation. The obtained results can provide the better understanding of the oxygen diffusion properties in the Ti-Al alloys and the oxidation of intermetallic systems. Furthermore, such knowledge of the diffusivity and its anisotropy is very important in engineering and to predict the influence of impurities on the limiting diffusion barriers and the oxygen diffusion related properties. The effect of impurities on the oxygen diffusion rate in the Ti-Al alloys will be considered in our forthcoming paper.

ACKNOWLEDGEMENTS

The present research has partly been supported by the Russian Foundation for Basic Research under Grant 18-03-00064_a, Institute of Strength Physics and Materials Science SB RAS (project III.23.2.8) and Tomsk State University Competitiveness Improvement Programme 2013–2020. Numerical calculations have been performed on the supercomputers at the National Research Tomsk State University and Lomonosov Moscow State University.

REFERENCES

1. Berdovsky, Y.N. (2008). *Intermetallics Research Progress.* New York: Nova Science.
2. Polmear, I. (2006). *Light Alloys: From Traditional Alloys to Nanocrystals*. Amsterdam: Butterworth-Heinemann.
3. Rahmel, A., & Spencer, P.J. (1991). Thermodynamic aspects of TiAl and $TiSi_2$ oxidation: The Al–Ti–O and Si–Ti–O phase diagrams. *Oxid. Met. 35*(1/2), 53–68.
4. Kofstad, P. (1988). *High Temperature Corrosion*. London: Elsevier Applied Science.
5. Maurice, V., Despert, G., Zanna S., Josso, P., Bacos M.-P., & Marcus. P. (2007). XPS study of the initial stages of oxidation of α_2-Ti_3Al and γ-TiAl intermetallic alloys. *Acta Mater.*, *55*, 3315–3325. DOI: 10.1016/j.actamat.2007.01.030
6. Umakoshi, Y., Yamaguchi, M., Sakagami, T., & Yamane, T. (1989). Oxidation resistance of intermetallic compounds Al_3Ti and TiAl. *J. Mater. Sci.*, *24*, 1599–1603.
7. Smialek, J.L., & Humphrey, D.L. (1992). Oxidation kinetics of cast $TiAl_3$. *Scripta Metall. Mater.*, *26*, 1763–1768.
8. Okafor, I.C.I., & Reddy, R.G. (1999). The oxidation behavior of high-temperature aluminides. *JOM* ,*51*(6), 35–40.

9. Becker, S., Schutze, M., & Rahmel, A. (1993). Cyclic-oxidation behavior of TiAI and of TiAI alloys. *Oxid. Met.*, *39*(1/2), 93–106.
10. Wang, J., Kong, L., Li, T., & Hiong, T. (2016). High temperature oxidation behavior of $Ti(Al,Si)_3$ diffusion coating on γ-TiAl by cold spray. *Trans. Nonferrous Met. Soc. China*, *26*, 1155–1162. DOI: 10.1016/S1003-6326(16)64214-0
11. Blöchl, P.E. (1994). Projector augmented-wave method. *Phys. Rev. B.*, *50*(24), 17953–17979. DOI: 10.1103/PhysRevB.50.17953
12. Kresse, G., & Joubert, J. (1999). From ultrasoft pseudopotentials to the projector augmented-wave method. *Phys. Rev. B.*, *59*(3), 1758–1775. DOI: 10.1103/PhysRevB.59.1758
13. Kresse, G., & Hafner, J. (1993). *Ab initio* molecular dynamics for open-shell transition metals. *Phys. Rev. B.*, *48*, 13115–13118. DOI: 10.1103/PhysRevB.48.13115
14. Kresse, G., & Furthmüller, J. (1996). Efficiency of ab-initio total energy calculations for metals and semiconductors using a plane-wave basis set. *Comput. Mater. Sci.*, *6*, 15–50. DOI: 10.1016/0927-0256(96)00008-0
15. Perdew, J.P., Burke, K., & Ernzerhof, M. (1996). Generalized gradient approximation made simple. *Phys. Rev. Lett.*, *77*(18) 3865–3868. DOI: 10.1103/PhysRevLett.77.3865
16. Henkelman, G., Uberuaga, B.P., & Jónsson, H. (2000). A climbing image nudged elastic band method for finding saddle points and minimum energy paths. *J. Chem. Phys.*, *113*(22), 9901–9904. DOI: 10.1063/1.1329672
17. Wei, Y., Zhou, H.B., Zhang, Y., Lu, G.-H., & Xu, H. (2011). Effects of O in a binary-phase TiAl–Ti_3Al alloy: From site occupancy to interfacial energetics. *J. Phys.: Condens. Matter.*, *23*(22), 225504. DOI: 10.1088/0953-8984/23/22/225504
18. Bakulin, A.V., Kulkova, S.E., Hu, Q.M., & Yang, R. (2015). Theoretical study of oxygen sorption and diffusion in the volume and on the surface of a γ-TiAl alloy. *J. Exp. Theor. Phys.*, *120*(2), 257–267. DOI: 10.1134/S1063776115020090
19. Shanabarger, M.R. (1998). Comparative study of the initial oxidation behavior of a series of titanium–aluminum alloys. *Appl. Surf. Sci.*, *134*(1–4), 179–186. DOI: 10.1016/S0169-4332(98)00196-2
20. Latyshev, A.M., Bakulin, A.V., Kulkova, S.E., Hu, Q.M., & Yang, R. (2016). Adsorption of oxygen on low-index surfaces of the $TiAl_3$ alloy. *J. Exp. Theor. Phys.*, *123*(6), 991–1007. DOI: 10.1134/S1063776116110133
21. Koizumi, Y., Kishimoto, M., Minamino, Y., & Nakajima, H. (2008). Oxygen diffusion in Ti_3Al single crystals. *Philos. Mag.*, *88*(24), 2991–3010. DOI: 10.1080/14786430802419135
22. Bakulin, A.V., Latyshev, A.M., & Kulkova, S.E. (2017). Absorption and diffusion of oxygen in the Ti_3Al alloy. *J. Exp. Theor. Phys.*, *125*(1), 138–147. DOI: 10.1134/S1063776117070019
23. Bertin, Y.A., Parisot, J., & Gacougnolle, J.L. (1980). Modèle atomique de diffusion de l'oxygène dans le titane α*. *J. Less-Common Met.*, *69*, 121–138.

SKĀBEKĻA DIFŪZIJAS PIRMPRINCIPU APRĒĶINI Ti-Al SAKAUSĒJUMOS

S. E. Kulkova, A. V. Bakulins, S. S. Kulkovs

K o p s a v i l k u m s

Projektora paplašinātā viļņa metode blīvuma funkcionālajā teorijā tiek izmantota, lai pētītu skābekļa difūziju intermetāliskajos Ti-Al sakausējumos. Rakstā parādīts, ka augstākās skābekļa absorbcijas enerģijas Ti-Al sakausējumos atbilst oktaedra Ti bagātām vietām, bet alumīnija klātbūtne tuvākajos reģionos ievērojami samazina skābekļa absorbcijas enerģiju sakausējumos. Tiek novērtētas migrācijas barjeras skābekļa difūzijai starp dažādām spraugām Ti-Al sakausējumu kristāla režģī. Pētījumā noteikti vēlamie migrācijas ceļi gar a un c asīm un ierobežojošas skābekļa difūzijas barjeras sakausējumos. Tiek apskatīta skābekļa difūzijas koeficienta atkarība no Ti-Al sakausējuma sastāva.

12.11.2018.

sciendo

LATVIAN JOURNAL OF PHYSICS
AND TECHNICAL SCIENCES
2018, N 6

DOI: 10.2478/lpts-2018-0041

AB INITIO CALCULATIONS OF CU_N@GRAPHENE (0001) NANOSTRUCTURES FOR ELECTROCATALYTIC APPLICATIONS

S. Piskunov, Y. F. Zhukovskii, M. N. Sokolov, J. Kleperis

Institute of Solid State Physics, University of Latvia,
8 Kengaraga Str., Riga, LV-1063, LATVIA
e-mail: piskunov@lu.lv

Substitution of fossil-based chemical processes by the combination of electrochemical reactions driven by sources of renewable energy and parallel use of H_2O and CO_2 to produce carbon and hydrogen, respectively, can serve as direct synthesis of bulk chemicals and fuels. We plan to design and develop a prototype of electrochemical reactor combining cathodic CO_2-reduction to ethylene and anodic H_2O oxidation to hydrogen peroxide. We perform *ab initio* calculations on the atomistic 2D graphene-based models with attached Cu atoms foreseen for dissociation of CO_2 and H_2O containing complexes, electronic properties of which are described taking into account elemental electrocatalytical reaction steps. The applicability of the model nanostructures for computer simulation on electrical conductivity of charged Cu_n/graphene (0001) surface is also reported.

Keywords: *Cu-decorated graphene, DFT, electronic properties, ESM*

1. INTRODUCTION

The electrocatalytic reduction of carbon dioxide is assumed to be reliable CO_2 converting process because it can be performed under low-pressure/temperature conditions, whereas relatively low cost of copper catalysts can facilitate the reduction pathway to hydrocarbons, e.g., ethylene [1]. However, the efficiency of these catalysts has still to be improved as large overpotentials are required for bulk Cu to reduce CO_2 to methane or ethylene while competing with the hydrogen evolution side reaction [2]. Within the last decade, a number of studies resulted in development of many interesting metal-containing catalysts. Nanostructures such as nanoparticles [3], and nanowires [4] have shown vastly improved activity or selectivity over bulk materials [5]. Recently, nanostructures derived from reduction of copper oxides have shown essentially improved efficiency of CO_2 reduction at lower overpotentials [6]. These materials were synthesized by using reduction of either thermally oxidized Cu or electrodeposited copper (I) oxide and showed improved current density, enhanced CO_2 reduction to carbon monoxide at low overpotentials and a partial suppression

of methane in favour of ethylene at higher overpotentials. Recently published data on plasma oxidized Cu-catalysts to produce oxides and a rough surface have shown Faradaic efficiency of 60 % for ethylene, which is the highest one achieved at the time of writing [7].

To provide a deeper insight into processes taking place during CO_2 reduction in the presence of nanostructured Cu catalyst, we plan to elaborate the method of electrochemical synthesis of Cu-decorated graphene. In this paper, we report the results of initial computer modelling steps of Cu_n@graphene nanostructure electronic properties. We are particularly interested in change of electronic properties with presence of applied voltage. This allows us to mimic current-voltage characteristics at the experimental electrochemical reactor for CO_2 reduction.

2. COMPUTATIONAL DETAILS

To investigate electronic properties of the slabs under study, we created corresponding models and performed first-principles calculations using a density-functional theory (DFT), as implemented in Quantum Espresso package [8]. Wave functions were represented in the plane wave basis set with energy cut-off achieving 40 Ry (544 eV). The Perdew-Becke-Ernzerhof (PBE) functional [9] was utilised for this aim. Core electron potentials were approximated within the projector augmented wave (PAW) method [10] that describes $2s^2 2p^2$ states for C (valence is four) and $4s^1 3d^{10}$ for Cu (valence is eleven). Simple monolayers were calculated using a corresponding supercell (SC) since Cu atop graphene required 5×5 SC underneath the single Cu atom or cluster. Monkhorst-Pack grid was used for Brillouin zone sampling [11], with different frequencies, depending on the system (for 5×5 graphene supercell, 6×6×1 grid was used).

Options required to investigate the charged systems properly are relatively limited. In this paper, to estimate the effect of applied voltage on the electronic structure, we used the effective screening medium (ESM) method [12]. In ESM, instead of having periodic boundary conditions in all three space directions, slab is considered to be sandwiched between semi-infinite media. Currently implemented options for media are vacuum-slab-vacuum, vacuum-slab-metal and metal-slab-metal.

In the current study, we cover ESM calculations (vacuum-slab-metal boundary conditions) of single graphene layer, graphene bilayer, Cu(111) monolayer as well as single Cu atom atop graphene. Calculations presented in this paper are building blocks and reference for future more complicated systems, as well as can serve for validation of the method. All properties of charged systems are presented with respect to the corresponding neutral system.

3. RESULTS AND DISCUSSION

In the beginning, we analyse the total charge per atom at different voltages as calculated with constant bias potential shown in Fig. 1. One could observe a linear dependence of total charge from voltage for all the investigated systems, with copper slab having a steeper line, meaning copper accumulates charge easier with voltage, which corresponds well with a known fact of copper superior conductivity.

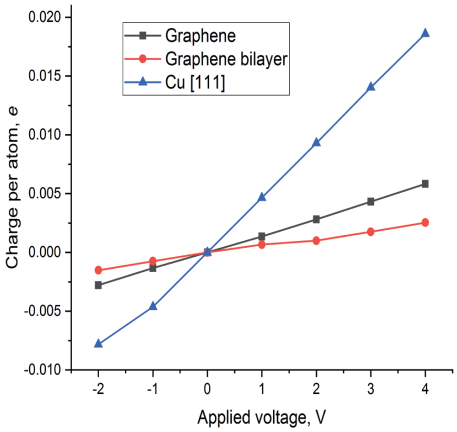

Fig. 1. Charge *per* atom versus applied voltage in different systems.

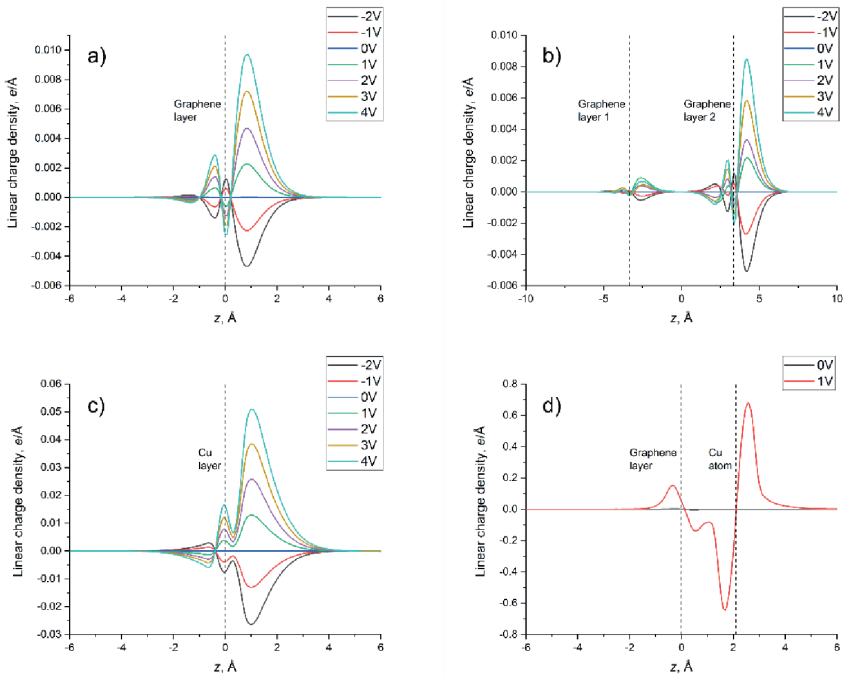

Fig. 2. Linear charge density versus vertical axis *z* for different systems: a) graphene monolayer; b) graphene bilayer; c) Cu [111] monolayer, d) single Cu atom atop graphene. Dashed lines denote *z* position of elements of a system. Vacuum and metal boundary conditions are not shown but are implied on the left and on the right, respectively (outside plotting range). Charge density is displayed with respect to the corresponding uncharged system.

Another thing that could be noticed is that the charge per atom of graphene bilayer is lower than on a monolayer. By comparing Figs. 2a and 2b, it can be concluded that the second graphene layer has a negligible effect on the charge density of the layer, closest to metal. To include interaction between layers, one has to use more sophisticated methods to estimate van der Waals forces, which are out of scope of this paper.

It is well seen that the charge dissipates from graphene and Cu surfaces similarly (Figs. 2a and 2c), reaching zero at about 3 Å outside the surface. Peaks for Cu densities have been found to be higher, although a care has to be taken when comparing these absolute numbers because a number of atoms in the system is different, 2 for graphene and 4 for Cu in this case.

When putting single Cu atom atop graphene, three sites were considered: directly above atom, above centre of a side of a hexagon or above centre of a hexagon. However, calculations yielded similar results with no site being favourable over another, so we put it above the centre of hexagon.

Constant bias potential calculations for this system are much more demanding and at the time of writing convergence of system at 1 V only was achieved (results are demonstrated in Fig. 2d). It could be clearly seen that the main charge of the system is around Cu atom, which might explain its catalytic properties.

4. CONCLUSIONS

In this study, we present results of large-scale first-principles calculations on the charged single graphene (0001) monolayer and bilayer, Cu(111) monolayer as well as single Cu atom atop graphene (0001) monolayer performed within the effective screening medium (ESM) method. The results demonstrate that the suggested model with ESM method is valid and can be used for modelling of Cu-decorated graphene. The acquired results will be used as building blocks for later modelling of larger systems that will include CO_2 and H_2O.

ACKNOWLEDGEMENTS

Funding from European Union's Horizon 2020 Research and Innovation Programme project under grant agreement No. 768789 is greatly acknowledged.

REFERENCES

1. Kuhl, K. P., Cave, E. R., Abram, D. N., & Jaramillo, T. F. (2012). New insights into the electrochemical reduction of carbon dioxide on metallic copper surfaces. *Energy Environ. Sci*., *5*, 7050–7059.
2. Zhang, Y.-J., Sethuraman, V., Michalsky, R., & Pereson, A. A. (2014). Competition between CO reduction and H evolution on transition-metal electrocatalysts. *ACS Catal.*, *4*, 3742–3748.
3. Reske, R., Mistry, H., Behafarid, F., Cuenya, B. R., Strasser, P. (2014). Particle size effects in the catalytic electroreduction of CO on Cu nanoparticles. *J. Am. Chem. Soc.*, *136*, 6978–6986.
4. Zhu, W. Zhang, Y.-J., Zhang, H., Lv, H., Li, Q., Michalsky, R., Peterson, A. A., & Sun, S. (2014). Active and selective conversion of CO_2 to CO on ultrathin Au nanowires. *J. Am. Chem. Soc.*, *136*, 16132–16135.
5. Mistry, H., Varela, A. S., Kuehl, S., Strasser, P., & Cuenya, B. R. (2016). Nanostructured electrocatalysts with tunable activity and selectivity. *Nat. Rev. Mater.*, *1*, 16009.

6. Ren, D., Deng, Y., Handoko, A. D., Chen, C. S., Malkhandi, S., & Yeo, B. S. (2015). Selective electrochemical reduction of carbon dioxide to ethylene and ethanol on copper (I) oxide catalysts. *ACS Catal.*, *5*, 2814–2821.
7. Mistry, H., Varela A. S., Bonifacio C. S., Zegkinoglou,I., Sinev, I., Choi, Y.-W., … Cuenya, B. R. (2016). Highly selective plasma-activated copper catalysts for carbon dioxide reduction to ethylene. *Nat. Commun.*, *7*, 12123.
8. Giannozzi, P., Baroni, S., Bonini, N., Calandra, M., Car., R., Cavazzoni, C., … Wentzcovitch, M. (2017). QUANTUM ESPRESSO: A modular and open-source software project for quantum simulations of materials. *J. Phys.: Condens. Matt.*, *29*, 465901.
9. Perdew, J. P., Burke, K., & Ernzerhof, M. (1996). Generalized gradient approximation made simple. *Phys. Rev. Lett.*, *77*, 3865–3868.
10. Kresse, G. J., & Jouber, D. (1999). From ultrasoft pseudopotentials to the projector augmented-wave method. *Phys. Rev. B*, *59*, 1758–1775.
11. Monkhorst, H. J., & Pack, J. D. (1976). Special points for Brillouin-zone integrations. *Phys. Rev. B*, *13*, 5188–5192.
12. Otani, M., & Sugino, O. (2006). First-principles calculations of charged surfaces and interfaces: A plane-wave nonrepeated slab approach. *Phys. Rev. B*, *73*, 115407.

CU_N/GRAFĒNA (0001) NANOSTRUKTŪRU *AB INITIO* APRĒĶINI ELEKTROKATALĪTISKAJIEM PIELIETOJUMIEM

S. Piskunovs, J. F. Žukovskis, M. N. Sokolovs, J. Kleperis

K o p s a v i l k u m s

Fosilo ķīmisko procesu aizstāšana, kombinējot atjaunojamās enerģijas avotu vadītās elektroķīmiskās reakcijas, un paralēli H_2O un CO_2 izmantošana oglekļa un ūdeņraža iegūšanai, attiecīgi, var kalpot kā neorganisko ķīmisko vielu un degvielu tieša sintēze. Mēs plānojam izstrādāt elektroķīmiskā reaktora prototipu, kas apvieno katodisko CO_2 reducēšanu līdz etilēnam un anodisko H_2O oksidēšanu līdz ūdeņraža peroksīdam. Mēs veicam ab initio aprēķinus ar atomu formāta 2D grafēna modeļiem ar pievienotiem Cu atomiem, kas paredzēti CO_2 un H_2O saturošu kompleksu disociācijai, kuru elektroniskās īpašības ir aprakstītas, ņemot vērā elementārās elektrokatalītiskās reakcijas pakāpes. Tika ziņots arī par modelēto nanostruktūru piemērotību uzlādētās Cu_N/grafēna (0001) virsmas elektriskās vadītspējas datormodelēšanai.

06.12.2018.

sciendo

LATVIAN JOURNAL OF PHYSICS
AND TECHNICAL SCIENCES
2018, N 6

DOI: 10.2478/lpts-2018-0042

EFFECT OF IN DOPING ON THE ZnO POWDERS MORPHOLOGY AND MICROSTRUCTURE EVOLUTION OF ZnO:In CERAMICS AS A MATERIAL FOR SCINTILLATORS

F. Muktepavela[1*], J. Maniks[1], L. Grigorjeva[1], R. Zabels[1],
P. Rodnyi[2], E. Gorokhova[3]

[1]Institute of Solid State Physics, University of Latvia,
8 Kengaraga Str., LV1063, Riga, LATVIA
*famuk@latnet.lv, manik@latnet.lv, lgrig@latnet.lv
[2] Peter the Great St.Petersburg State Polytechnic University,
29 Polytekhnicheskaya Str., 195251, Saint-Petersburg, RUSSIA
Rodnyi@tuexph.stu.neva.ru
[3] Scientific and Production Association S.I.Vavilov
State Optical Institute
36 Babushkina Str., 192171, Saint-Petersburg, RUSSIA
E.Gorokhova@rambler.ru

Transparent ZnO ceramics are of interest for use as material for high-efficiency fast scintillators. Doping ZnO ceramics in order to improve complex of their properties is a promising direction. In the present research, the role of indium in the ZnO nanopowders surface interactions and in the change of microstructures and photoluminescence (PL) characteristics of sintered ceramics is considered. Undoped and 0.13 wt% In doped ZnO ceramics are obtained by hot pressing sintering. It has been found that indium leads to the transition of initially faceted ZnO particles to rounded, contributing to good sintering with formation of diffusion active grain boundaries (GBs). Unlike ZnO ceramics, ZnO:In ceramics microstructure is characterised by the trans-crystalline mode of fracture, faceted GBs with places of zig-zag forms and predominant distribution of In at the GBs. Such indium induced modifications of GBs promote removal of point defects and reduce PL parameter $\alpha = I_{def}/I_{exc}$ in comparison with the undoped ceramics. Results characterise ZnO:In ceramics with improved GBs properties as a prospective material for scintillators.

Keywords: *grain boundaries, hot pressing sintering, In doped ZnO ceramics, photoluminescence, ZnO powders*

1. INTRODUCTION

ZnO as a multifunctional material continues to be the subject of thorough study for many years. The interest in ZnO remains high due to potential applications of various ZnO nanostructures [1], [2] and due to new opportunities for nanocrystalline films, coatings and ceramics obtained by more efficient technologies [3]–[5]. Possibilities of using ZnO as a polycrystalline material have stimulated theoretical and experimental research in the field of surface energy, features in surface states and grain boundaries (GBs) in ZnO systems [6], [7].

These findings are important not only for conductive transparent ZnO thin films but to an even greater extent for sintered ZnO ceramics based on nanopowders. Transparent ZnO ceramics are of interest for use as high-efficiency fast scintillator. This requires high intensity of radioluminescence or photoluminescence (PL) exciton peak (3.36 eV), negligible point defect associated "green" peak (2.45 eV), subnanosecond decay time and absence of GBs brittleness [8], [9]. To ensure such properties, a high-quality microstructure without micropores and with the minimal number of point defects should be formed during the sintering of ceramics. As known, the sintering process is determined not only by technological parameters but also by the powder interaction in the initial state and the behaviour of GBs at the stage of grain growth [10]. Sintering of ZnO ceramics presents certain difficulties due to the variety of ZnO nanopowder morphological forms and their tendency to quickly agglomerate, which can lead to the residual pores, high concentration of point defects and GBs brittleness [11], [12]. The method of hot pressing ZnO powder activates volume diffusion, which helps eliminate the porosity of the ceramics; however, as we have shown earlier, it is practically difficult to eliminate the presence of point defects even during hot pressing [12]. On the other hand, it is known that introduction of donor impurities such as gallium or indium into the composition can alter the properties of ZnO nanocrystals and films [3], [13]. In [14] for the first time ZnO:In transparent ceramic has been obtained by hot pressing sintering in vacuum. It has been shown that the indium doping leads to the increase of the intensity of X-ray luminescence excitonic band and ensures photonic response with a subnanosecond decay time. To understand the nature of In effect on ZnO:In ceramics properties, in the present research we consider the influence of indium on the powder interaction and microstructure formation during sintering.

2. EXPERIMENTAL PART

Commercial zinc oxide powder (99.9995 %, "*Alfa AESAR"*, USA) was used to obtain ceramics. The indium in the form of indium oxide (UHP, Russia) was introduced by mechanical mixing with the original ZnO powder during 40 min at 293K. Ceramics of undoped and 0.13 wt% In doped ZnO were fabricated by uniaxial hot pressing sintering in vacuum at temperature 1150 °C and P = 100–200 MPa for 60 min [14]. Microstructures were investigated by scanning electron microscopy (SEM, LYRA, Tescan, Oxford, HV:15-40 kV) with energy dispersive X-ray spectroscopy (EDS, Eagle III XPL), transmission electron microscopy (TEM, FEI, Tecnai, GF20) and optical microscopy (Eclipse L150, Nicon). Photoluminescence (PL) was mea-

sured under YAG: Nd laser excitation (266 nm, 2 ns pulse) at 293 K. The ratio value of "defect" to excitonic PL intensities ($\alpha = I_{def}/I_{exc}$) was measured by using 125 ns time gate. The luminescence was recorded with a phonon counting head (HAMAMATSU H8259) and photon counting board Fast Com Tech module P 7887 with 500 channels and minimal time bins of 250 ps. The monochromator MDP-3 was used for spectral measurements.

3. RESULTS AND DISCUSSION

3.1. Powder Morphology

Figures 1, a,b,c are TEM and SEM images showing the morphology of undoped ZnO powders. The original ZnO powder (Fig. 1,a,b,c) is characterised by a considerable inhomogeneity; it contains faceted particles: nanograins (d_g = 25–50 nm), nanorods (d_g = 20 nm, l = 100 nm) and thin elongated nanobelts (l = 100–200 nm). Strong agglomeration of these powder particles is observed – in the form of chains, rings and relative large platforms. The aggregation of individual nanorods occurs by orienting the outer facets, mostly prismatic (1010) non-polar low energy planes (shown in Fig. 1,b with arrows).

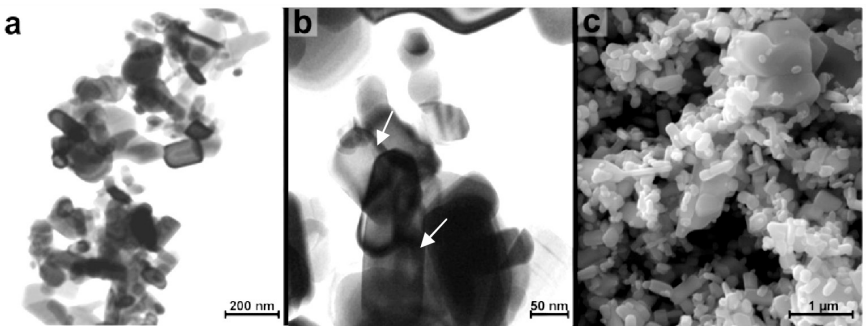

Fig. 1. TEM (a, b) and SEM (c) images of initial (original) ZnO powder.

Addition of indium leads to a significant change in the original ZnO powder morphology. As can be seen from Fig. 2 a,b,c, the general trend under the influence of indium is the rounding of original ZnO faceted particles. Large ring-shaped aggregates or large platforms in this case are almost absent.

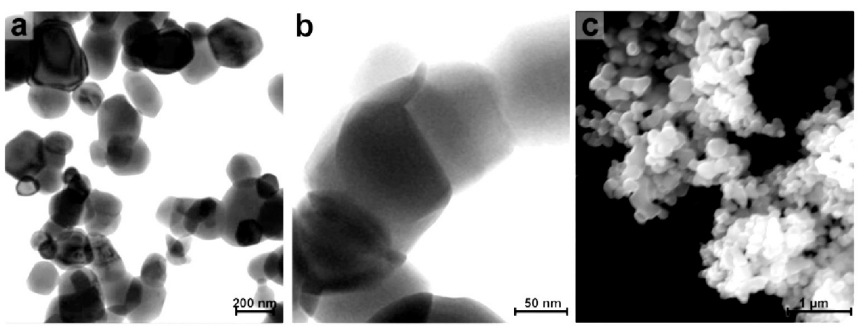

Fig. 2. TEM (a, b) and SEM (c) images of ZnO:In 0.13wt% powders.

An unique non-faceted ZnO:In aggregates are formed, in which roughed GBs and triple junctions are visible. Thus, it has been found that already during the mixing of powders indium facilitates a transition of initial faceted ZnO particles to rounding. As it is known, rounded particles are preferable for sintering due to spontaneous adhesion determined by the surface self-diffusion and formation of diffusion active high angle GBs on the contact [4], [10], [17].

It should be noted that the ability of indium to change the shape of ZnO nanoparticles during contacting has not been investigated. However, the reaction between ZnO and In_2O_3 at 1100 °C has been studied in [18], where phase diagram of ZnO-In_2O_3 is presented. Thus, it is known that ZnO can interact with In *via* solid state reactions forming compounds ZnO+$Zn_7In_2O_{10}$. In our case, these interactions occur on the contact surfaces, so it is necessary to take into account the thermodynamic features of the ZnO surface planes. In many theoretical studies [6], [7], [19] the calculations reveal that the surface energy γ of Zn-0001 polar plane is higher (γ_{zn} = 2.0 J/m^2) than that of O-000$\bar{1}$(γ_o = 1.6 J/m^2). Zn-0001 surface is more unstable and active for interaction with such additive elements as Ga and In. From this point, the interactions of In_2O_3 –ZnO occur via mechanical alloying [20] on the edges of Zn-0001 polar plane contacting with the non-polar plane. As a result, there is a violation of the atomic arrangement that leads to the faceting-rounding transitions [17] of powder surfaces and formation of stable ZnInO compound in local contact places.

3.2. Microstructure of Ceramics

In Fig. 3, a,b,c the microstructure of undoped ZnO ceramics is presented. The micrograph of undoped ceramics shows recrystallized isometric grains with sizes d_g = 7–25 μm (Fig. 3,a). Consideration of fracture characteristics, as the most informative and important for sintered ceramics, has shown that fracture of undoped ZnO ceramics (Fig. 3,b,c) has mainly brittle intergranular mode. Here, in some places, the presence of fractured substructure and elongated grains are visible. Fracture of them occurs by cleavage (Fig. 3,c). The heterogeneity of the initial powder structure is manifested in this ceramics.

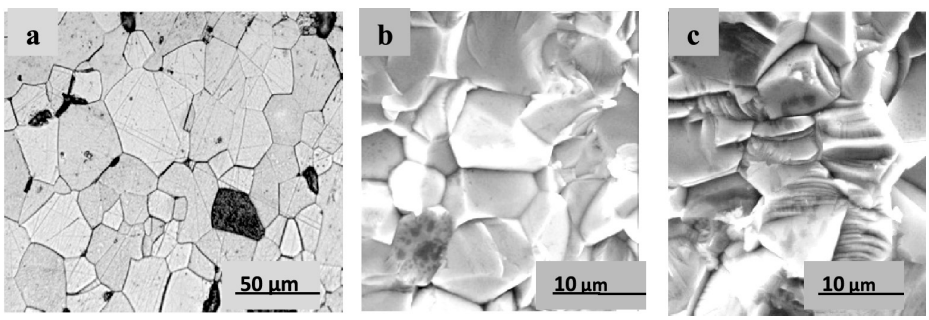

Fig. 3. Micrographs of etched external surface (a), and SEM images of fracture surfaces (b),(c) of sintered undoped ZnO ceramics.

Completely different unusual microstructures have surfaces in In doped ceramics (Fig. 4, a,b,c). In general, the microstructure is smaller (d_g = 2–5 μm) than for undoped ceramics. Furthermore, in the structure there are faceted GBs, some grains

are elongated (d = 5 μm, l = 10–15 μm), contain many twins and zig-zag forms of GBs. The presence of the zig-zag GBs in ZnO:In ceramics prevents the rapid spread of cracks along GB [21]. Confirmation of this is the fracture transcrystalline mode in In doped ceramics (Fig. 4,c) compared with undoped.

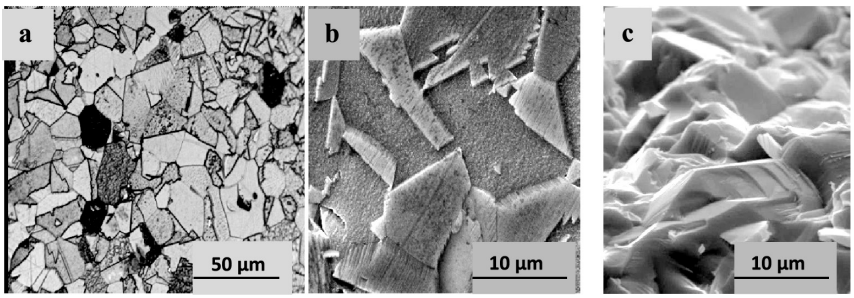

Fig. 4. Micrographs (a) and SEM image (b) of etched external surfaces, SEM image of fracture (c) of sintered 013 wt% In doped ZnO ceramics.

Indium induced zig-zag edges of polar (Zn-0001) planes in the nanobelts and ZnO films were observed in [22], [23]. In our case, zig-zag form appearance reflects the evolution of powder interfaces, discussed above, and are associated with the presence of ZnOIn compounds in the local places of GBs, which lead to the different mobility of GB structural elements during sintering [24]. The relative EDS data obtained from fracture surfaces of the ZnO: In samples showed that EDS signals of indium were obtained only in the area with high density of zig-zag and faceted GBs of fine grains, where O/Zn/In ratio is In-0.45, Zn-84.18, O-15.38 (wt%). Stoichiometric ZnO crystal exhibits the ratio O-19.99, Zn -80.3 (wt %) [2]. Therefore, GBs in ZnO:In ceramics have excess amount of Zn and In that confirms the presence ZnOIn compound.

Moreover, zig-zag GBs forms prevent the grain growth [10], [21] that, in turn, promotes the rapid removal of point defects during sintering due to shorter paths of vacancies from the source inside the grain to the sinks at faceted GBs.

This should primarily be reflected in PL results.

3.3. Photoluminescence of Ceramics

Figure 5,a,b shows the PL spectra for undoped ZnO and ZnO:In ceramics obtained at 300K. For both investigated ceramics excitonic at λ =380 nm and "green" at λ = 480–520 nm bands PL were observed. These bands are well known for single crystals, nanopowders, coatings and ceramics. Undoped ceramics has the wide "green" (defect associated) band at λ = 480–520 nm, whereas defect associated luminescence in ZnO:In is negligible. The ratio of defect to excitonic intensities at the same time range is an important parameter for ceramic characterization. The calculated values of this parameter $\alpha = I_{def}/I_{exc}$ at 300K are 1.2 and 0.08 for undoped and indium doped ZnO ceramics, respectively. Therefore, the indium doping of ZnO ceramics leads to the decrease of PL α parameter in 15 times. Here it can be noted that calculated from [14] for 0.13 wt% In doped ZnO ceramics X-ray luminescence parameter α was even decreased by 85 times compared with undoped.

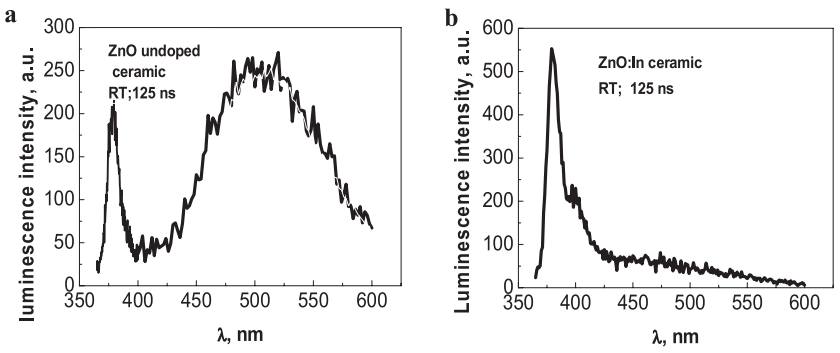

Fig. 5. The photoluminescence spectra of undoped ZnO (a) and ZnO:0.13 %wt In ceramics (b).

In the undoped ZnO ceramics disseminated vacancies remain inside grains due to slow volume diffusion processes at 1150 ºC and large distance to probable sinks in the coarse grain microstructure. In the ZnO:In ceramics faceted GBs with the local zig-zag forms contribute to a shorter path of vacancies from the source inside the grain to sink at the boundaries. Thus, the doping of ZnO with 0.13 wt% indium facilitates the elimination of point defects that is very important for a short decay time of scintillators [8].

4. CONCLUSIONS

A comparative analysis showed that doping of ZnO with 0.13 wt% indium changes all investigated properties of ZnO ceramics. During the mixing of powders indium induces a faceting-rounding transition of initially ZnO particles promoting good sintering with formation of diffusion active high angle GBs. This phenomenon is caused by the thermodynamics of In with ZnO contact interaction at the edges of Zn-0001 polar plane, leading to the stable ZnOIn compound formation in local places of GBs. The effect of In doping on the ZnO ceramics microstructure is mainly concerned with modifications of grain boundaries during sintering, including formation of fine grains, faceted GBs with zig-zag forms and excess amount of Zn and In.

Such improved GBs provide reliable ways to remove point defects and significantly reduce the PL parameter I_{def}/I_{exc}. Results characterise 0.13 %wt In doped ZnO ceramics as a prospective material for fast scintillators.

ACKNOWLEDGEMENTS

The present research has been supported by the Project ERANET RUS_ ST#2017-051(Latvia) and #18-52-76002 (Russia).

REFERENCES

1. Klingshirn, C. F., Meyer, B. K., Waag, A., & Hoffmann, A. (2010). Zinc oxide. From fundamental properties towards novel applications. *Springer Series in Materials Science. 120.* Springer, Heidelberg.

2. Ozgur, U., Alivov, Y I., Liu, C., Teke A., Reshchikov, M. A., Dogan, S. ... Morkoc, H. (2005). A comprehensive review of ZnO materials and device*s. J. App.Phys. 98,* 043011.
3. Zhang, Z., Du, J., Li, B., Zhang, S., Hong, M., Zhang, X. …Zhang, Y. (2017). Ultrathin strain gated field effect transistor based on In-doped ZnO nanobelts. *APL Materials 5,* 086111.
4. Lu, K. (2008). Sintering of nanoceramics. *Intern. Mater. Rev*. *53*, 21–38.
5. Polyakov, B., Dorogin, L., Lohmus, A., Romanov, A., & Lohmus, R. (2012). In situ measurement of the kinetic friction of ZnO nanowires inside a scanning electron microscope. *Appl. Surf. Sci. 258,* 3227–3231.
6. Wilson, H. F., Tang, C., & Barnard, A. S. (2016). Morphology of zinc oxide nanoparticles and nanowires: Role of surface and edge energies. *Phys. Chem. C*, *120*, 9498.
7. Huber, S. E., Hellström, M., Probst, M., Hermansson, K., & Broqvist, P. (2014). Large-scale SCC-DFTB calculations of reconstructed polar ZnO surfaces. *Surf. Sci. 628,* 50–61.
8. Wilkinson, J., Ucer, K.B., & Williams, R.T. (2005). The oscillator strength of extended exciton states and possibility for very fast scintillators. *Nucl. Instr. and Methods. Phys. Res. A. 537*, 66–70.
9. Rodnyi, P. A., Chernenko, K. A., Gorokhova, E. I., Kozlovskii, S.S., Khanin, V.M., & Khodyuk, I.V. (2012). Novel scintillation material – ZnO transparent ceramics. *IEEE Trans. Nucl. Sci. 59(5)*, 2152–2155.
10. Kelly, J. P., & Graeve, O A. (2013). Effect of powder characteristics on nanosintering sintering mechanisms of convention nanodensification and field assisted processes. *Sintering*, 57–95.
11. Muktepavela, F., Zabels, R., Sursajeva, V., Grigorjeva, L., & Kundzins, K. (2012). The role of nanopowder particle surfaces and grain boundary defects in the sintering of ZnO ceramics. *IOP Conf. Ser. Mater. Sci. Eng*. *38*, 012016.
12. Muktepavela, F., Grigorjeva, L., Kundzins, K., Gorokhova, E., &Rodnyi, P. (2015). Structure, nanohardness and photoluminescence of ZnO ceramics based on nanopowders. *Phys. Scr. 90* 094018.
13. Yanagida, T., Fujimoto, Y., Yoshikawa, A., & Maeo, S. (2010). Scintillation properties of In-doped ZnO with different In concentrations. *IEEE Trans. Nucl. Sci. 57*(3)*,* 1325–1328.
14. Gorokhova, E. I., Eron'ko, S. B, Kul'kov, A., Oreshchenko, E. A., Simonova, K. L., Chernenko, K. A. ... Wieczorek, H. (2015). Development and study of ZnO:In optical scintillation ceramic. *J. Opt. Technol. 82*(12)*,* 837–842.
15. Sohn, J. I., Hong, W-K, Lee, S., Lee, S., Ku, J., Park, Y. J. ... Kim, J.M. (2014). Surface energy-mediated construction of anisotropic semiconductor wires with selective crystallographic polarity. *Sci. Rep.4,* 5680.
16. Klinger, L., & Rabkin, E. (2010). Sintering of fully faceted crystalline particles. *Intern. J. Mater.Res.*, *101* (1), 75–83.
17. Yoon, Y., & Cho, Y., K. (2005) Roughening transition of grain boundaries in metals and oxides. *J. Mater. Sci.*, *40,* 861–870.
18. Moriga, T., Edwards, D.D., Mason, T.O., Palmer, G.B., Kenneth Poeppelmeier, R., Schindler, J.L. … Nakabayashi, I. (1998). Phase Relationships and Physical Properties of Homologous Compounds in the Zinc Oxide–Indium Oxide System. *J. Am. Ceram. Soc., 81, 5,* 1310-1316.
19. Tang, C., Spencer, M.J. S., & Barnard, A. S. (2014). Activity of ZnO polar surfaces: An insight from surface energies*. Phys. Chem. Chem. Phys.*, *16,* 22139–22144.
20. Muktepavela, F., Bakradze, G., & Stolyarova, S. (2006). Effect of mechanoactivation on interfacial interaction in metal/oxide systems. *Defect and Diffusion Forum, 249*, 263–268.

21. Cahn, R. W. (ed.). (1965). *Physical Metallurgy*. *8*. Amsterdam: North Holland.
22. Oba, F., Sato, Y., Yamamoto, T., Ohta, H., Hosono, H., & Ikuhara, Y. (2005). Effect of boundary plane on the atomic structure of [0001] Σ 7 tilt grain boundaries in ZnO. *J. Mater. Sci. 40,* 3067.
23. Fan, H. J., Fuhrmann, B., Scholz, R., Himcinschi, C., Berger, A., Leipner, H. … Zachatias, M. (2006). Vapour-transport-deposition growth of ZnO nanostructures: Switch between c-cxial wires and a-axial belts by indium doping. *Nanotechnology, 17,* 231–239.
24. Sursaeva, V, Gornakova, A., & Muktepavela, F. (2014). Grain boundary ridges slow down grain boundary motion: In-situ observation. *Mater. Lett. 124,* 241735.
25. Chen, I-W, & Wang, X.-H. (2000). Sintering dense nanocrystalline oxide without final stage grain growth. *Nature, 404,* 168–171.

INDIJA IETEKME UZ ZnO PULVERA MORFOLOĢIJU UN MIKROSTRUKTŪRAS EVOLŪCIJU ZnO:In KERAMIKĀ KĀ SCINTILĀTORU MATERIĀLU

F. Muktepāvela, J. Maniks, L. Grigorjeva, R. Zabels,
P. Rodnyi, E. Gorokhova

K o p s a v i l k u m s

Caurspīdīgas ZnO un ZnO:In keramikas izpelnās interesi pielietojumiem augstas efektivitātes scintilatoros. Šim nolūkam nepieciešama augsta fotoluminiscences (FL) eksitonu pīķa intensitāte, iespējami vāja ar defektu stāvokļiem saistītā „zaļā" josla ZnO keramikās ar augstu mikrostruktūras kvalitāti. Šajā darbā ar karstās presēšanas pie 1500 ^{o}C iegūtas ZnO un ZnO:0,13 wt % In keramikas pētītas, izmantojot SEM, TEM un FL metodes. Noskaidrots, ka jau pulveru sajaukšanas stadijā In veicina sākotnēji fasetēto daļiņu pāreju uz noapaļotu stāvokli, kas sekmē saķepināšanos un lielleņķu graudu robežu (GR) ar lielu difūzijas spēju veidošanos. Indija inducēta keramikas mikrostruktūras evolūcija noved pie fasetētas, vietām zigzaga GR. Šī GR modifikācija bremzē graudu augšanas procesus, nodrošinot noteces vietas punktvieda defektiem un FL parametra $\alpha = I_{def}/I_{exc}$ (attiecība starp defektu un eksitonu FL intensitāti) ievērojamu samazināšanu, salīdzinot ar nedopeto ZnO keramiku. Rezultāti liecina, ka ZnO:0.13 wt%In keramiku ar uzlabotām GR var izmantot kā materiālu scintilatoriem.

26.11.2018.

sciendo

LATVIAN JOURNAL OF PHYSICS
AND TECHNICAL SCIENCES
2018, N 6

DOI: 10.2478/lpts-2018-0043

LUMINESCENCE PROPERTIES AND DECAY KINETICS OF Mn^{2+} AND Eu^{3+} CO-DOPANT IONS IN $MgGa_2O_4$ CERAMICS

A. Luchechko[1,a], Ya. Zhydachevskyy[2,3], D. Sugak[2,b], O. Kravets[1], N. Martynyuk[2], A.I.Popov[4,c], S. Ubizskii[2], A. Suchocki[3,5]

[1] Ivan Franko National University of Lviv,
107 Tarnavskogo St., Lviv 79017, UKRAINE

[2] Lviv Polytechnic National University, 12 Bandera St.,
Lviv 79646, Ukraine

[3] Institute of Physics, Polish Academy of Sciences,
32/34 Al. Lotnikow, Warsaw 02-668, POLAND

[4] Institute of Solid State Physics, University of Latvia, LATVIA

[5] Institute of Physics, University of Bydgoszcz, Weyssenhoffa 11,
Bydgoszcz 85-072, POLAND

E-mail: [a]andriy.luchechko@lnu.edu.ua,
[b]dm_sugak@yahoo.com, [c]popov@latnet.lv

The $MgGa_2O_4$ ceramics co-doped with Mn^{2+} and Eu^{3+} ions were synthesized via a high-temperature solid-state reaction technique. The samples with various Eu^{3+} concentrations were characterised using high-resolution photoluminescence (PL) spectroscopy. The PL spectra show weak matrix emission in a blue spectral region with dominant excitation band around 380 nm. Manganese ions are highly excited deeply in UV region and exhibit emission band peaked at 502 nm. The Eu^{3+} ions show characteristic f-f excitation and emission lines. The energy transfer between host defects and activator ions was observed. Luminescence decay curves of Mn^{2+} and Eu^{3+} emission showed complex kinetics with both Eu^{3+}-ion concentration and excitation wavelength changes.

Keywords*: energy transfer, europium (Eu^{3+}) and manganese (Mn^{2+}) ions, decay kinetics, magnesium gallate $MgGa_2O_4$, photoluminescence*

1. INTRODUCTION

Complex oxides with crystalline structures of perovskite, garnet and spinel have many important properties that determine their successful application in science and technology, in such areas as ferroelectricity, semiconductor electronics, optoelectronics, luminescence and radiation technology etc. [1]–[11]. In particular,

transition metal or rare earth ion doping of these materials creates excellent emitting phosphor materials [11]–[27]. Among these ions, the Mn^{2+} and Eu^{3+} ions are known as the main sources of green and red light emission, respectively. Thus, such materials are often used in display technologies, such as field emission displays, vacuum fluorescent displays etc. [12], [14].

At the same time, the Eu^{3+} ions are active in crystal sites with low point symmetry caused by the large degree of inversion of the spinel structure (e.g., magnesium gallate $MgGa_2O_4$) and other structural perturbations. In order to obtain efficient phosphors, the coexistence of tetrahedral and octahedral cation sites is the key factor for host materials [15]. As far as we know, there are only a few reports of photoluminescence (PL) decay investigations in $ZnGa_2O_4$: Eu^{3+} spinel obtained by different methods [12], [14]. Simultaneously, no detailed study has been reported about decay profiles and energy transfer process in $MgGa_2O_4$: Eu^{3+}. Only Tsai et al. 2006 [28] reported about the decay curve of $^5D_0 \rightarrow {}^7F_2$ transition of $MgGa_2O_4$: 5% Eu^{3+} nanopowder. Moreover, no PL decay kinetics investigations have been yet reported for $MgGa_2O_4$ co-doped with Mn^{2+} and Eu^{3+}.

In the present research, the high-resolution PL excitation and emission spectra, as well as decay characteristics of Mn^{2+} and Eu^{3+} co-doped magnesium gallate ceramics are presented.

2. EXPERIMENTAL DETAILS

The synthesis had been carried out via high-temperature solid-state ceramic technique from simple oxide powders of at least 4N grade of purity. The powders were mixed with the stoichiometric composition in an agate mortar for 6 h with further pressing. The obtained tablets were annealed at 1200 °C for 8 hours in the air. The concentration of Mn^{2+} was set constant at 0.05 mol.% and concentration of Eu^{3+} ions was changed from 2 mol.% to 4 mol.%. The phase and structure analysis were described earlier [13], [29].

PL and appropriate PL excitation (PLE) spectra were measured at room temperature using a Horiba/Jobin-Yvon Fluorolog-3 spectrofluorometer with a 450 W continuous xenon lamp as an excitation source, while a Hamamatsu R928P was used as a detector. The measured PLE spectra were corrected for the xenon lamp emission spectrum. The PL spectra were corrected for the spectral response of the spectrometer system. The PL decay kinetics was recorded using an Edinburgh FS5-MCS spectrofluorometer equipped with a 5 W/ms Xenon flash lamp.

3. RESULTS AND DISCUSSION

PL excitation spectra of $MgGa_2O_4$ co-doped with 0.05 mol.% Mn^{2+} and 4 mol.% Eu^{3+} ions registered at several emission wavelength are shown in Fig. 1a. Two excitation bands of the matrix emission in the $MgGa_2O_4$ ceramics co-doped with Mn^{2+} and Eu^{3+} ions were observed in the UV and near UV regions of spectra. Deeper UV excitation band peaking around 260 nm shows a lower intensity with respect to near UV band at about 380 nm. The excitation spectrum of Mn^{2+} ion registered at

502 nm demonstrates intense excitation deeply in the UV spectral region indicating the recombination process as it corresponds to the region of fundamental absorption edge (E_g = 5 eV) [28]. The tail in the exitation of manganese ions from 260 to 320 nm shows that the charge transfer ($O^{2-} \rightarrow Mn^{2+}$) also occurs [1], [13], [14].

The europium ions are excited with the charge transfer from oxygen anions to Eu^{3+} ions (240–340 nm) and the *4f-4f* intra-shell transitions of Eu^{3+} ions corresponding to the sharp lines (350–420 nm) under 615 nm registration [13], [29]. The remarkable sharp declines of the excitation intensities in the range of *f-f* lines on the excitation spectra registered at 440 nm and 502 nm indicate that the energy transfer occurs through excitation mechanisms between host defects and activator ions.

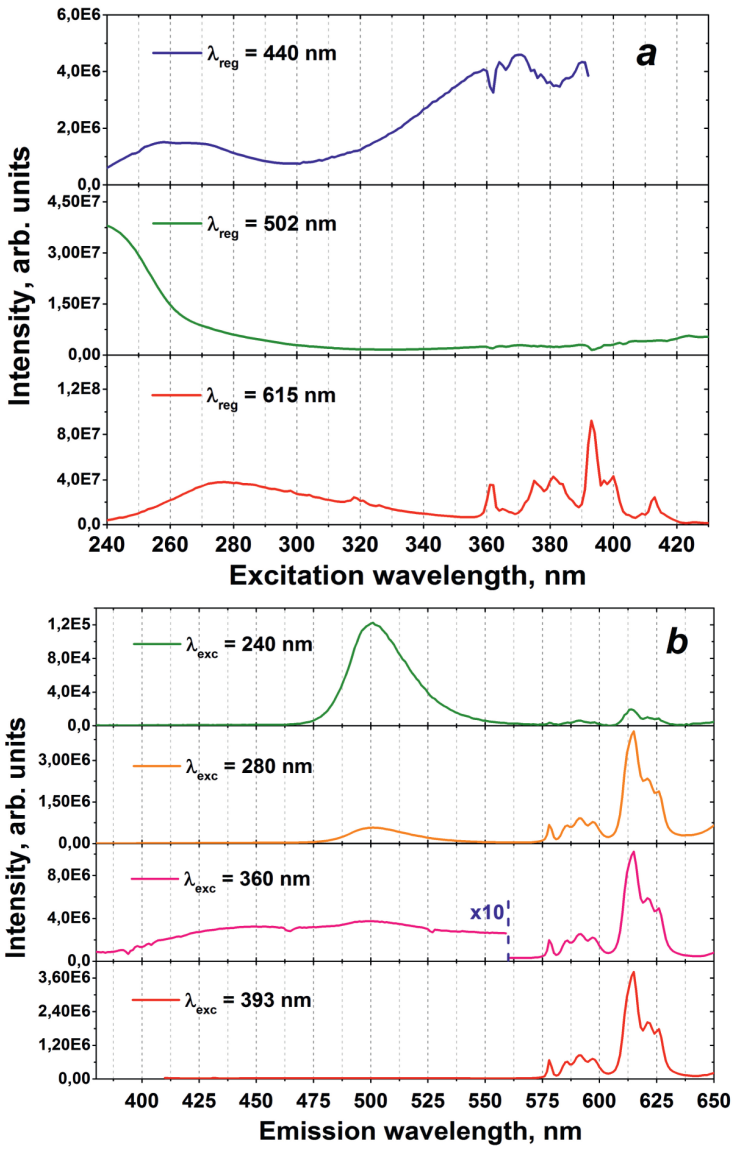

Fig.1. Photoluminescence excitation (a) and emission (b) spectra of $MgGa_2O_4$ co-doped with 0.05 mol.% Mn^{2+} and 4 mol.% Eu^{3+} ions.

PL spectra of $MgGa_2O_4$ co-doped with 0.05 mol.% Mn^{2+} and 4 mol.% Eu^{3+} ions at different excitations are shown in Fig. 1b. The luminescence of $MgGa_2O_4$:Mn^{2+},Eu^{3+} is represented by the UV-blue host emission and activator ions in green and orange-red regions, respectively. The host luminescence originating from structural defects is clearly seen under 360-nm excitation [29]. The decline of the host emission intensity at about 393 and 463 nm is due to reabsorption by Eu^{3+} ions in the near-surface ceramics layer [13]. The emission of Mn^{2+} ions peaked at ~ 502 nm is the most intense at 240-nm excitation due to the efficient energy transfer from $MgGa_2O_4$ host to the Mn^{2+} ions [30]. At the same time, the orange-red emission of Eu^{3+} ions is the most intense under the 280, 380 and 393 nm excitations. Only dominant emission of Eu^{3+} ions is obtained at 393-nm excitation, which corresponds to $^7F_0 \rightarrow {}^5L_6$ electron transitions in the activator ions. Note that redistribution of the emission intensities in hyperfine structure of $^5D_0 \rightarrow {}^7F_2$ transitions, and a change in excitation wavelength is found as well.

All PL decay curves of $MgGa_2O_4$:Mn^{2+}, x Eu^{3+} excited at 240 nm and monitored at 505 nm can be fitted with double-exponential function: $I(t) = A_1 exp(-t/\tau_1) + A_2 exp(-t/\tau_2)$, where I(t) is the emission intensity, A_1 and A_2 are the weighting constants, τ_1 and τ_2 are the fast and slow decay components of the luminescence lifetimes, respectively. The typical curve for $MgGa_2O_4$:Mn^{2+}, 4 mol% Eu^{3+} is shown in Fig. 2a. It has been established that fast and slow components are at about 3.2 and 5.6 ms, respectively. Moreover, the lifetime constants of manganese ions weakly depend on the europium concentration. One can assume that one of the components is related to Mn^{2+} ions in the tetrahedral sites of the spinel structure and the another with manganese ions near structural defects or in distorted tetrahedral sites, for example, by oxygen vacancies. At the same time, to reveal the nature of the fast and slow components more detailed investigation is needed. It should also be noted that $MgGa_2O_4$: Mn^{2+} shows a single-exponential decay with τ = 7.1 ms at the excitation in the region of *d-d* intraband transitions of Mn^{2+} ions [30].

The PL decay curves of Eu^{3+} ions have been measured at a different excitation wavelength in the emission peak at 615 nm. Figure 2b shows the PL decay curves of Eu^{3+} ions in $MgGa_2O_4$ ceramics co-doped with 0.05mol% Mn^{2+} and 2-8% Eu^{3+} at 393 nm excitation that corresponds to the *f-f* transitions in Eu^{3+} ions. The decay curves were also fitted using the double exponential function. The values of a lifetime are presented in Table 2. The lifetime decreases with growth of the Eu^{3+} ion doping level. Short component changes from 0.31 to 0.14 ms and a long one from 1.98 to 0.77 ms.

Table 1

Decay Profiles of Double Exponential Fitting of $MgGa_2O_4$ Co-doped with 0.05 mol.% Mn^{2+} and 2-8 mol.% Eu^{3+} Ions at 615 nm Registration and Excition 270 nm

x mol.% Eu^{3+} ions	τ_1, ms	A_1, %	τ_2, ms	A_2, %	Adj.R^2
2	0.26	94.8	0.98	5.2	0.99981
4	0.19	77.2	0.78	22.8	0.99983
6	0.17	72.4	0.76	27.6	0.99952
8	0.11	80.6	0.58	19.4	0.99934

Table 2

Decay Profiles of Double Exponential Fitting of $MgGa_2O_4$ Co-doped with 0.05 mol.% Mn^{2+} and 2-8 mol.% Eu^{3+} Ions at 615 nm Registration and Exitation 393 nm

x mol.% Eu^{3+} ions	τ_1, ms	A_1, %	τ_2, ms	A_2, %	Adj.R^2
2	0.31	98.3	1.98	1.7	0.99875
4	0.25	81.5	0.82	18.5	0.99914
6	0.18	67.1	0.79	32.8	0.99896
8	0.14	52.4	0.77	47.3	0.99862

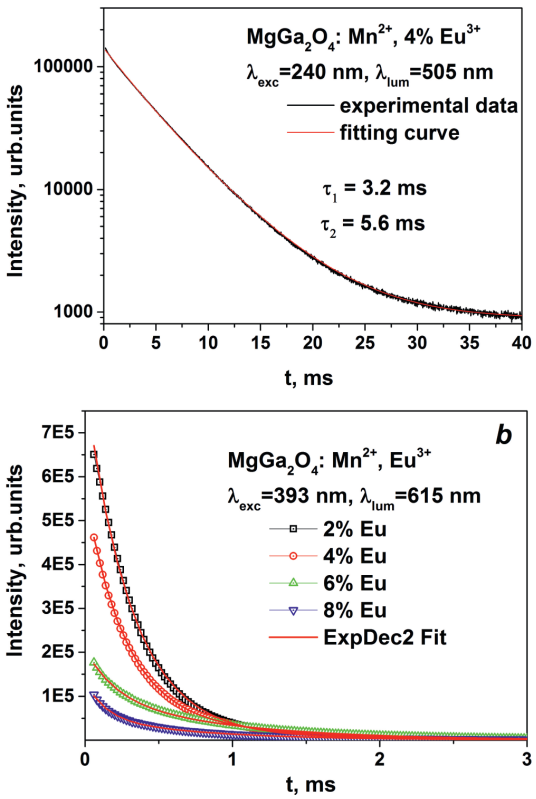

Fig. 2. Decay kinetic curves of Mn^{2+} ions (a) and Eu^{3+} ions (b) in magnesium gallate spinel.

The decay curves for $ZnGa_2O_4$: 4%Eu^{3+} nanospheres and $MgGa_2O_4$: 5%Eu^{3+} nanopowders were fitted with a single exponential function with lifetimes 0.472 ms [12] and 0.934 ms [28], respectively. At the same time, the double exponential function was used for the decay profiles in $ZnGa_2O_4$: Eu^{3+} nanopowders [14], [15]. It was suggested [28] that only one mechanism was involved in the luminescence process, and most of the Eu^{3+} ions occupied distorted octahedral sites in the $Mg_xZn_{1-x}Ga_2O_4$ crystallites. In $MgGa_2O_4$: Mn^{2+}, Eu^{3+}, the decay kinetics was more complicated, which suggested involvement of at least two mechanisms in the luminescence process. The fast component was tentatively related to Eu^{3+} located on grain boundaries. The second process could be attributed to the Eu^{3+} ions in crystallite bulk.

Table 3

Decay Profiles of Double Exponential Fitting of $MgGa_2O_4$ Co-doped with 0.05 mol.% Mn^{2+} and 4 mol.% Eu^{3+} Ions at Different Excitations and 615 nm Registration

λ_{exc}, nm	τ_1, ms	A_1, %	τ_2, ms	A_2, %	Adj.R^2
240	0.14	80.4	0.78	19.6	0.99943
270	0.19	77.2	0.78	22.8	0.99983
300	0.20	76.3	0.74	23.7	0.99978
380	0.23	78.9	0.76	21.1	0.99962
393	0.25	81.5	0.82	18.5	0.99914

4. CONCLUSIONS

The excitation spectrum of Eu^{3+}-emission shows dominance of *4f-4f* transitions over the charge transfer band despite it is also very intense. Emission spectra demonstrate that the $^5D_0 \rightarrow {}^7F_2$ transitions of Eu^{3+} ions in the orange-red spectral region are the most intense ones. The energy transfer from the host and Mn^{2+} ions to Eu^{3+} ions has been demonstrated by the excitation/emission spectra as well as PL decay curves. The luminescence decay time of Mn^{2+} emission has been determined to be ~ 4.7 ms and independent of Eu^{3+} ions concentration. The emission decay profiles of Eu^{3+} emission ions in $MgGa_2O_4$ co-doped with 0.05 mol.% Mn^{2+} and 2-8 mol.% Eu^{3+} ions have been observed to be non-exponential, depending on different europium concentrations and excitation wavelengths.

ACKNOWLEDGMENTS

The research has partly been supported by the Ukrainian Ministry of Education and Science within the Latvian–Ukrainian Joint Research Project (LV-UA/2016/1 in Latvia, and M/.8-2018 in Ukraine) and the project DB/RIDER (No. 0117U004443). A. Luchechko gratefully acknowledges a grant from the Institute of Physics PAS for a research visit to the institute, while A.I. Popov has been supported by project LZP-2018/1-0214 from the Latvian Council of Science.

REFERENCES

1. Brik, M. G., Suchocki, A., & Kaminska, A. (2014). Lattice parameters and stability of the spinel compounds in relation to the ionic radii and electronegativities of constituting chemical elements. *Inorganic chemistry*, *53*(10), 5088–5099.
2. Suchocki, A., & Powell, R.C. (1988). Laser-induced grating spectroscopy of Cr^{3+}-doped $Gd_3Ga_5O_{12}$ and $Gd_3Sc_2Ga_3O_{12}$ crystals. *Chemical Physics*, 128(1), 59–71.
3. Matkovski, A., Durygin, A., Suchocki, A., Sugak, D., Neuroth, G., Walrafend, F., ... Solski, I. (1999). Photo and gamma induced color centers in the $YAlO_3$ and $YAlO_3$:Nd single crystals. *Optical Materials*, 12(1), 75–81.

4. Dimza, V., Popov, A. I., Lāce, L., Kundzins, M., Kundzins, K., Antonova, M., & Livins, M. (2017). Effects of Mn doping on dielectric properties of ferroelectric relaxor PLZT ceramics. *Current Applied Physics*, *17*(2), 169–173.
5. Porotnikova, N. M., Anan'ev, M. V., & Kurumchin, E. K. (2011). Effect of defect structure of lanthanum manganite on oxygen exchange kinetics and diffusion. *Russian Journal of Electrochemistry*, *47*(11), 1250–1256.
6. Porotnikova, N. M., Eremin, V. A., Farlenkov, A. S., Kurumchin, E. K., Sherstobitova, E. A., Kochubey, D. I., & Ananyev, M. V. (2018). Effect of AO segregation on catalytical activity of $La_{0.7}A_{0.3}MnO_{3\pm\delta}$ (A= Ca, Sr, Ba) regarding oxygen reduction reaction. *Catalysis Letters*, *148*(9), 2839–2847.
7. Piskunov, S., Isakoviča, I., & Popov, A. I. (2018). Electronic structure of Mn^{3+}_{Al} and Mn^{2+}_{Al}-doped $YAlO_3$: Prediction from the first principles. *Optical Materials*, *85*, 162–166.
8. Klym, H., Ingram, A., Shpotyuk, O., Hadzaman, I., Solntsev, V., Hotra, O., & Popov, A. I. (2016). Positron annihilation characterization of free volume in micro-and macro-modified $Cu_{0.4}Co_{0.4}Ni_{0.4}Mn_{1.8}O_4$ ceramics. *Low Temperature Physics*, *42*(7), 601–605.
9. Piskunov, S., Isakoviča, I., & Popov, A. I. (2018). Atomic structure of manganese-doped yttrium orthoaluminate. *Nuclear Instruments and Methods in Physics Research Section B: Beam Interactions with Materials and Atoms*, *434*, 6–8.
10. Porotnikova, N.M., Ananyev, M.V., Eremin, V.A., Molchanova, N.G., & Kurumchin, E.K. (2016). Effect of acceptor substitution in perovskites $La_{1-x}A_xMnO_{3\pm\delta}$ (A = Ca, Sr, Ba) on the kinetics of interaction of gas-phase oxygen. *Russian Journal of Electrochemistry, 52(*8), 717–722.
11. Zhydachevskyy, Ya., Martynyuk, N., Popov, A.I., Sugak, D., Bilski, P., Ubizskii, S., … Suchocki, A. (2018). Thermally induced fading of Mn-doped YAP nanoceramics. *Journal of Physics: Conference Series*, 987(1), 012009.
12. Zhang, Y., Wu, Z., Geng, D., Kang, X., Shang, M., Li, X., … Lin, J. (2014). Full color emission in $ZnGa_2O_4$: Simultaneous control of the spherical morphology, luminescent, and electric properties via hydrothermal approach. *Advanced Functional Materials*, *24*(42), 6581–6593.
13. Luchechko, A., & Kravets, O. (2017). Novel visible phosphors based on $MgGa_2O_4$-$ZnGa_2O_4$ solid solutions with spinel structure co-doped with Mn^{2+} and Eu^{3+} ions. *Journal of Luminescence*, *192*, 11–16
14. Duan, X., Yu, F., & Wu, Y. (2012). Synthesis and luminescence properties of $ZnGa_2O_4$ spinel doped with Co^{2+} and Eu^{3+} ions. *Applied Surface Science*, *261*, 830–834.
15. Huo, Q., Tu, W., & Guo, L. (2017). Enhanced photoluminescence property and broad color emission of $ZnGa_2O_4$ phosphor due to the synergistic role of Eu^{3+} and carbon dots. *Optical Materials*, *72*, 305–312.
16. Polisadova, E. F., Vaganov, V. A., Stepanov, S. A., Paygin, V. D., Khasanov, O. L., Dvilis, E. S., ... Kalinin, R. G. (2018). Pulse cathodoluminescence of the impurity centers in ceramics based on the $MgAl_2O_4$ spinel. *Journal of Applied Spectroscopy*, *85*(3), 416–421.
17. Martynyuk, N.V., Ubizskii, S.B., Buryy, O.A., Becker, K.D., & Kreye, M. (2005). Optical *in-situ* study of the oxidation and reduction kinetics of Yb-substituted YAG epitaxial films. *Physica Status Solidi C: Conferences*, *2*(1), 330–333.
18. Zhydachevskii, Y., Syvorotka, I.I., Vasylechko, L., Sugak, D., Borshchyshyn, I.D., Luchechko, A.P., … Suchocki, A. (2012). Crystal structure and luminescent properties of nanocrystalline YAG and YAG:Nd synthesized by sol-gel method. *Optical Materials, 34*(12), 1984–1989.

19. Luchechko, A., Kravets, O., Kostyk, L., & Tsvetkova, O. (2016). Luminescence spectroscopy of $Eu^{3+}$and Mn^{2+} ions in $MgGa_2O_4$ spinel. *Radiation Measurements, 90*, 47–50.
20. Kirm, M., Feldbach, E., Lushchik, A., Lushchik, Ch., Maaroos, A., Savikhina, & T. (1997). Luminescent materials with photon multiplication. *Optical Inorganic Dielectric Materials and Devices* (eds. A. Krumins, D.K. Millers, A. Sternberg, J. Spigulis) *Proc. SPIE*, *2967*, 18–23.
21. Lushchik, A., Lushchik, Ch., Kotlov, A., Kudryavtseva, I., Maaroos, A., Nagirnyi, V., & Vasil'chenko, E. (2004). Spectral transformers of VUV radiation on the basis of wide-gap oxides. *Radiation Measurements*, *38*(4–6), 747–752.
22. Lushchik, A., Lushchik, C., Popov, A.I., Schwartz, K., Shablonin, E., & Vasil'chenko, E. (2016). Influence of complex impurity centres on radiation damage in wide-gap metal oxides. *Nuclear Instruments and Methods in Physics Research Section B: Beam Interactions with Materials and Atoms*, *374*, 90–96.
23. Lushchik, A., Dolgov, S., Feldbach, E., Pareja, R., Popov, A. I., Shablonin, E., & Seeman, V. (2018). Creation and thermal annealing of structural defects in neutron-irradiated $MgAl_2O_4$ single crystals. *Nuclear Instruments and Methods in Physics Research Section B: Beam Interactions with Materials and Atoms*, *435,* 31–37.
24. Kravets, O.P., Lys, R.M., Tsvetkova, O.V., Luchechko, A.P., & Pavlyk, B.V. (2018). Thermally stimulated luminescence and thermally stimulated depolarization currents in $MgGa_2O_4$ spinels. *Journal of Physical Studies, 22(1)*, 1602.
25. Luchechko, A., Kravets, O., & Syvorotka, I.I. (2017). Optical and luminescence spectroscopy of zinc gallate phosphors codoped with manganese and europium ions. *Spectroscopy Letters, 50(7)*, 404–410.
26. Luchechko, A., Kravets, O., Tsvetkova, O. (2017). Structure and optical-lumenescent characteristics of $Mg_{1-x}Zn_xGa_2O_4$: Mn^{2+} ceramics. *Journal of Nano- and Electronic Physics, 9(1)*, 01003.
27. Valiev, D., Khasanov, O., Dvilis, E., Stepanov, S., Polisadova, E., & Paygin, V. (2018). Luminescent properties of $MgAl_2O_4$ ceramics doped with rare earth ions fabricated by spark plasma sintering technique. *Ceramics International*, *44*(17), 20768–20773.
28. Tsai, B. S., Chang, Y. H., & Chen, Y. C. (2006). Preparation and luminescent characteristics of Eu^{3+}-activated $Mg_xZn_{1-x}Ga_2O_4$ nanocrystals. *Journal of Alloys and Compounds*, *407*(1–2), 289–293.
29. Luchechko, A., & Kravets, O. (2017). Synthesis and luminescent properties of magnesium gallate spinel doped with Mn^{2+} and Eu^{3+} ions. *Physica Status Solidi C*, *14*(1–2), 1600146.
30. Luchechko, A., Zhydachevskyy, Y., Maraba, D., Bulur, E., Ubizskii, S., & Kravets, O. (2018). TL and OSL properties of Mn^{2+}-doped $MgGa_2O_4$ phosphor. *Optical Materials*, *78*, 502–507.
31. Takesada, M., Osada, M., & Isobe, T. (2009). Glycothermal synthesis and photoluminescence of $MgGa_2O_4$: Mn^{2+} nanophosphors: Comparison to $ZnGa_2O_4$: Mn^{2+} nanophosphors. *Journal of the Electrochemical Society*, *156*(5), J97–J101.

AR Mn^{2+} UN Eu^{3+} JONIEM LEĢĒTĀS $MgGa_2O_4$ KERAMIKAS LUMINISCENCES ĪPAŠĪBAS UN SABRUKŠANAS KINĒTIKA

A. Lučečko, J. Žudačevski, D. Sugaks, O. Kravets, N. Martiņuks,
A.I.Popovs, S. Ubizski, A. Sučocki

K o p s a v i l k u m s

Ar Mn^{2+} un Eu^{3+} joniem leģētā $MgGa_2O_4$ keramika tika sintezēta, izmantojot augstas temperatūras cietvielu reakcijas metodi. Paraugi ar dažādām Eu^{3+} koncentrācijām tika raksturoti, izmantojot augstas izšķirtspējas fotoluminiscences (PL) spektroskopiju. PL spektrā ir redzama vāja matricas emisija zilajā spektra zonā ar dominējošo ierosmes joslu ap 380 nm. Mangāna joni ir ierosināti UV zonā un izstaro emisijas joslu, kuras maksimums ir 502 nm. Eu^{3+} joniem ir raksturīgas f-f ierosmes un emisiju līnijas. Tika novērota enerģijas pārnese starp matricas defektiem un aktivatora joniem. Mn^{2+} un Eu^{3+} emisijas luminiscences dzesēšanas līknes parādījušas sarežģītu kinētiku saistībā ar Eu^{3+} jonu koncentrācijas un ierosmes viļņa garuma izmaiņām.

07.12.2018.

sciendo

LATVIAN JOURNAL OF PHYSICS
AND TECHNICAL SCIENCES
2018, N 6

DOI: 10.2478/lpts-2018-0044

INTRODUCTION OF ENERGY SAVING PRINCIPLES: TECHNOLOGIES AND AWARENESS, LATVIAN EXPERIENCE

A.Mutule, J.Teremranova

Institute of Physical Energetics,
11 Krivu Str., Riga, LV-1006, LATVIA
E-mail: energija@edi.lv

The article presents an overview of the current situation of awareness of the Latvian citizens in the field of state-of-the-art energy-saving technologies. The authors present a wide range of data obtained as a result of a survey on the attitude of residents to new technologies and readiness to follow the development trends of a smart city.

The article contains the analysis and recommendations for improving the efficiency of introducing new energy-saving and energy-efficient technologies into each household in order to create the most favourable conditions for the implementation of long-term plans for the development of smart cities in Latvia.

Keywords*: citizen awareness, efficient energy use, energy consumption, energy control and management, energy saving technologies, smart city, survey*

1. INTRODUCTION

Urbanisation is becoming an integral part of our century, and according to various forecasts, in the coming decades 60 %–80 % of the population of the planet will move to the cities. This process is largely of objective character because it promotes an increase in a productive activity in many areas, and at the same time helps solve social economic problems of the society. It goes without sayingthat one of the most important directions in the development of smart cities is electric engineering, in particular, the introduction of economical, effective technologies of power and heat generation, increasing the safety of power and heat supply in the cities, introduction of energy saving technologies and application of materials and equipment ensuring longer terms of their explotation. Energy consumption is also closely relatedto business activity and living standards of the population. The more aware and independently acting inhabitants of the cities are, the higher level of energy efficiency will be reached [1].

Furthermore, the 21st century is characterised by information technology explosion; many of the technologies offer their own solution to the task of competent and economical consumption of energy resources. Nowadays, web platforms are generally available that enable evaluation of quantitave and qualitative indicators of one's consumption and choice of the most appropriate variant of management of resource consumption and their cost.

Therefore, a successful model of a smart city can be based on the balanced long-term strategy of electric engineering development or activity plan aimed at stable electric engineering for a smart city, which in essence is also the starting point for future iniciatives as an integrated tool for infrastructure development. Actually, the way to the smart city starts with a clear plan that includes ambitious goals, concept of necessary legislative amendments and, of course, indicators for measuring progress [2], [3].

2. BACKGROUND

As shown in paper [4], consumers sufficiently contribute to achieving flexibility in energysystems by changing the amount and way of energy consumption, which can promote a growth of stability of the whole energy system and decrease of the system load in peak hours. For that purpose, understanding and use of the technologies available in the market is crucially important, as well as understanding of one's contribution to promoting the growth of renewablesshare and ensuringa more flexible energysystem. According to the market research conducted by Lattelecom in 2017 [5], despite the fact that electric energy market in Latvia was opened on 1 January 2015, currently 97 % of households in Latvia are using services of the main trader and only 3 % of the population exploit new possibilities of reducing power consumption expenses by changing their consumption tariff and/or changing the trader.

The authors of [6] point to the fact that effective interaction with consumers is crucial for the electricity supplier, who installs smart meters and systems, and suggests using different tariffs of energy consumption, including dynamic tariff, i.e., variable price each month in accordance with the price at the electricity exchange. Commonly, consumers do not have or have insufficient experience of interaction with smart meters, hour-to-hour data provided by smart meters and control of energy consumption in their households.

The problem is compounded by the fact that a huge number of new technologies are entering the market, including on-line programs to control a power consumption rate and load, new equipment and information systems, Web portals, calculators and software to compare and control energyconsumption.All the above requires customer attention, willingness to study and master new technologies, and readiness to use them to control their own resources. Some utility servicesare introducing new time tariffs, e.g., dynamic tariff, i.e., variable price each month in accordance with the price at the electricity exchange, load management as well as other user-oriented programs that help them to study their power consumption models, understand how the programs will affect the tariffs, and in the long run, make validated decisions regarding the use of energy and controlling it. These programs turn only to be ef-

fective when customers have a good understanding of costs, profits and value of the offer, and decide to play a more significant role in the management of their energy consumption and expenses.

As experience shows, most frequent and informative communication with customers takes place either personally or by phone or, most frequently, in the electronic form using automatic messages and replies, as well as using the internet, web tools, social networks, TV and other tools used for advertising. Often, several communication methods are required to establish successful interaction. Teaching and incorporating new clients have to be performed on a regular basis. The authors have studied issues of the Latvian population's flexibility and adaptivity to iniciatives of energy efficient use of resources, and also examined the causes and ways to influence awareness and acceptance of new iniciatives by the country's inhabitants.

3. REVIEW OF ENERGY RESOURCES IN LATVIA

According to the data of Central Statistical Bureau (CSB) of Latvia [7], electric energy consumption in households (in percentage) increases every year (see Fig. 1).

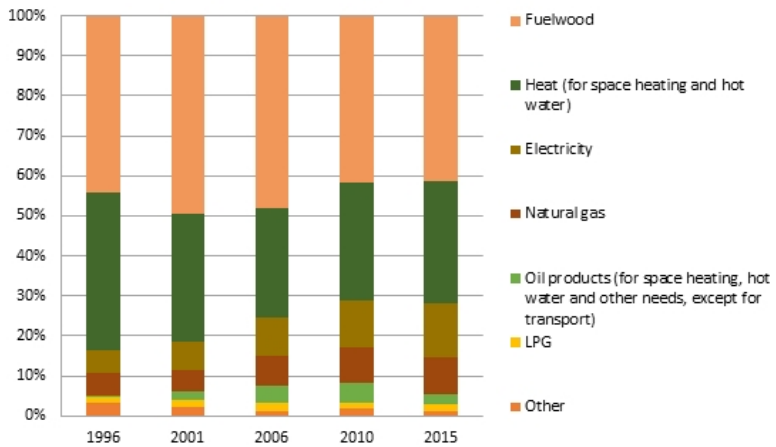

Fig. 1. Changes in the structure of energy consumption in households, by CSB.

As of 2015, energy consumption in households constituted 14 % of total energy consumption, excluding transport, while total household expenditure on energy consumed (see Fig. 2) was 40 % of the cost of total energy consumed in households. Since 2001, an average price of electric energy for households has risen nearly three times.

Since 2010, the electricity cost in the total expenditure has increased by 34 %, while the costs of other energy resources have diminished or have not changed [7]. While the total indicator of the final consumptionof energy in Latvia has a tendency to decrease, energy consumption in households grows every year. In 2016, it constituted 28 % of the final energy consumption in Latvia.

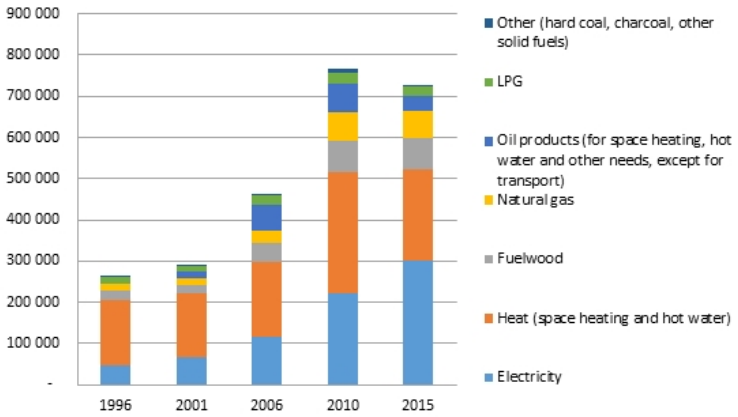

Fig. 2. Total household expenditure on energy consumed (in thousands of euros), by CSB.

According to CSB data, average consumption of electricity per household has not changed a lot: 2008 kwh/year in 2010 and 2185 kwh/year in 2015, which can serve as an indicator that under the continued growth of electric appliances and equipment that consume energy in households, efficient energy use is an important and necessary condition for the Latvian inhabitants.

4. ANALYSIS OF THE NEEDS AND AWARENESS OF ELECTRICITY CUSTOMERS IN LATVIA

To clarify the picture of the Latvian inhabitants'awareness in the field of innovations and possibilities of a smart city, an anonymous survey has been developed. Another aimof the survey has beento study the existingbeliefs and habits in the sphere of energy resource management that promote or impede the use ofnew intelligent potentialitiesof a smart city.The survey included topics like information sufficience on the specified theme, confidence in the information gained from different sources, issues of personal values and priorities, issues of finance as a motivator, as well as studying what else can serve asa motivator for changes, and the presence of possible limitations on changing the behaviour to ecological, stable and energy saving.

In the course of the survey, these trends have been discovered that are fundamental for understanding customer response to possible changes:

- A third of the respondentshave no idea about such a notion as a smart city and have never heard about the iniciatives aimed at constructing a smart city (Fig. 3, (a));
- More than half of respondents have admitted that they have no idea about any projects oriented towards "smart" energy resource consumption in their city (Fig. 3, (b)).

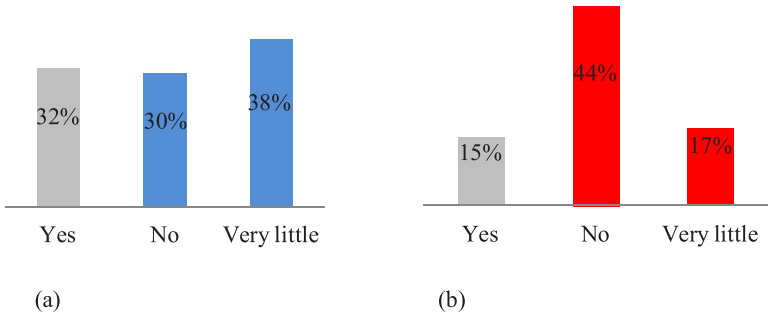

Fig. 3, (a) and (b). Answers to questions about smart city.

The data obtained reflect an unsufficient level of the Latvian inhabitants' informativity about iniciatives implemented in the sphere of a smart city. This is the gap that should be filled first of all by solving the issue about information sources that the Latvian inhabitants use and trust.

The above-mentioned consideration is supported by the fact that 4/5 of the respondents have positively answered a question "Are you interested in saving energy?" This is a very good dynamics for promoting projects and iniciatives aimed at raising the intellectuality of the Latvian cities and saving energy in case ofappropriate material delivery and information provision. Moreover, 80 % of inhabitants consider it important to have up-to-date technologies at home, whereas 20 % do not care about it.

To promote training and informing the inhabitants about the latest achievements in the field of electric engineering and energy resource saving, we have first of all to find out what the current state of affairs is and what issues are important and necessary not only from the viewpoint of the government, administration and legislative references, but also from the point of view of ordinary people, each of which is an energy consumer. It is also essential to search out which topics motivate their willingness to accept the noveltiesand develop by following modern technologies and trends, and which ones cause non-acceptance, as well as to find out the reason forsuch behaviour. These circumstances could be different within different countries, and may even differin cities withinacountry. This is a detailed study of the circumstances that can promote further successful organisation and development of a city wishing to be "smart".

Respondents have also been asked a question: What is your attitude to energy saving technologies? Their replies show the level of awareness existing in Latvia nowadays:

- The most numerous group of respondents (about 60 %) have responded that they do know about energy saving technologies and use them a little bit;
- 20 % of respondents have stated that they are aware of energy saving technologies but do not use them. While working with that kind of customers, it is crucially important to find out the causes, why a person refuses to try to apply "smart" technologies. Quite frequently, the focal point is distrust and/or willingness to follow a customary way of living and consumption;

- A bit less than 1/5 inhabitants are not aware of energy saving but wish to know about it. In this case, it is important to study furtherthe ways people use information and what sources should be used to exchange information and communicate with them. Say, mobile applications and information in social networks would suit young people best, whereas for people of ripe age personal contact could be determinant.
- Only a very small group of people (about 3 %) have responded that they neither know about such technologies nor wish to know about them. Actually, this can only be evidence that a special approach is required to contact this kindof people to awake their interest in energy saving issues.

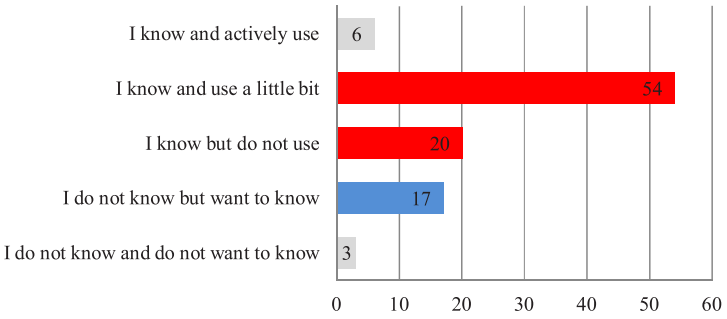

Fig.4. Respondent's attitude to energy saving technologies.

In Fig. 4, two groups of people marked can be considered, correspondingly, in red and blue colour. Respondents out of the red group do know about new technologies but due to some reasons do not use them or use them very little. Therefore, simply distributing information about new projects and innovations in the field of energy saving it is impossible to solve the issue of informeduse of the technologies above by inhabitants. Additional studies are required to more precisely define the reasons as well as motivation that will work just in the specified group of people. Here, the research discussed in [4] should be mentioned whose authors have conducted considerable research aimed at clearing up what information sources customers trust, as well as what the form is in which information not only can be taken into consideration but also starts to be used in households.

On the other hand, respondents ascribed to the "blue" group, i.e., those who wish to know but know nothing about smart energy and smart consumption, due to some reasons areuninformed about energy saving and introduction of new technologies despite all advertising handled and existing within the iniciatives of a smart city. Most probably, this gives evidence that training information has to find new channels of reaching clients.Again, this is a topic of thorough study of such group of customers, specifically, it is important to find out who enters the group, what the age-related characteristicsare, what information sources they are accustomed to use and where they would be ready to obtain and take into consideration information, offers and iniciatives on energy saving technologies.

It should also be noted that despite the fact that an absolute majority of respondents are interested in energy resource saving, their vision how to implement it dif-

fers: three fourths of inhabitants prefer to use at home a new energy saving technology that itself will care about smart consumption of resources after the adjustment, whereas one fourth of inhabitants prefers manual everyday correction of equipment that consumes energy resources in order to diminish their consumption.

The topic of the Latvian citizens' motivation to use energy saving technologies is quite interesting and important (the respondents could tick several techniques that are close and motivating for them). A question: "What would make you to more frequently use energy saving technologies?" has been answered as follows:

- 34 % of respondents have chosen the example of neighbours/friends/acquaintances;
- 32 % of inhabitants stand for public companies that would explain the advantages of new technologies;
- the overhelming majority of respondents, i.e., 63 % are sure that they would benefit from vividly represented savings of energy and money;
- 13 % of respondents would be motivated by an example of state public figures;
- For 39 % of respondents, awareness that they will promote nature and earth resource preservation for their offspring is important.

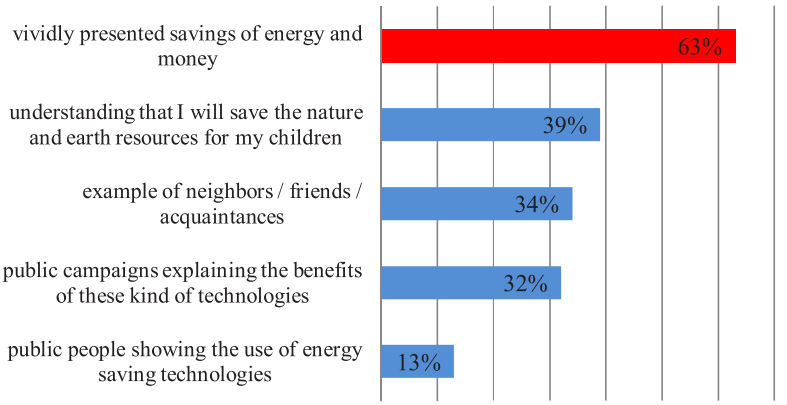

Fig.5. Motivation to use energy saving technologies.

All the aforementioned topics motivating the Latvian inhabitants to save resources as well as their distribution percentage deserve further attention and study with a view to organise effective introduction of new energy saving technologies in our life. As pointed in [8], a majority of approaches to reaching stable energetic behaviour consider people in the context of their wish to acquire and enlarge their wealth and property. Although a social context plays a great role in the way how people think and behave, they do not realise it frequently. We are members of different social groups and societies that can affect our behaviour and persuasion in using innovative technologies and energy efficiency attitudes.

Financial issue definitely also contributes to the influence of the Latvian inhabitants' choice on the use of innovative energy saving technologies.

- 46 % of respondents would be ready to use the new technologies provided they would pay off within 1–2 years;
- 39 % would be ready to wait for the payback period of 3–4 years;
- 12 % have made investments in new technologies or will be ready to do so if the payoff period is within 5–10 years.

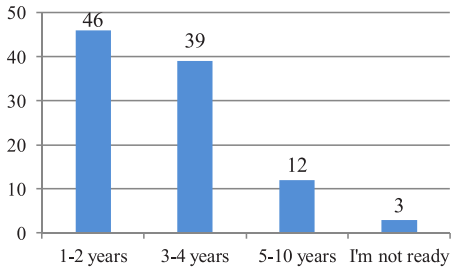

Fig. 6. Readiness to pay for new technologies: "I am ready to use the new technology if it pays off".

Another vector of research has been directed towards finding out how much money a person is ready to pay for new technologies every month knowing that they help one save energy and lead to the enhancement of an ecological situation in the country. As a result, it has been found that (see Fig. 7):

- 17 % are ready to pay € 1–2 per month;
- 28 % – € 3–4 per month;
- 36 % – € 5–10 per month;
- 11 % – more than € 10 per month;
- 8 % are not ready at all to invest money that way.

In other words, it can be argued that 97 % of people in Latvia are ready to pay for new technologies.

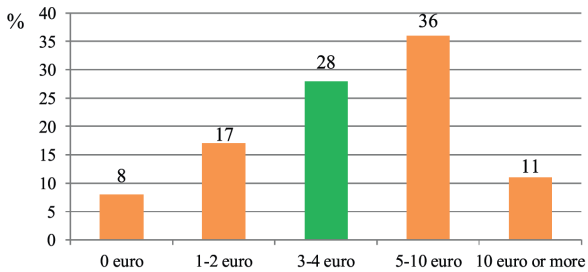

Fig. 7. "How much money would you agree to pay monthly for new technologies in your home, knowing that they will help to save energy and improve the environment?"

Basically, the Latvian inhabitants are ready to invest in new technologies € 3 – € 10 monthly provided they are sure that the investment would ensure energy, and respectively, money saving (48 % of all respondents).

In the course of the survey, the authors have also examined existing perception stereotypes of the Latvian inhabitants regarding new possibilities ofcontrolling and saving energy, for instance, readiness/unreadiness to change a service trader or to

pass on to another mode of energy consumption and payment, as well as willingness and readiness to model their consumption by using mobile applications with game elements (see Fig. 8). In the survey, respondents could point several choices that were closest to them. Survey results are summarised below.

- For a third of respondents, stability and predictability are the key factors and they wish to change nothing. This is a serious claim for long-term and gradual working with this kind of customers aimed at having an opportunity to change habits of these people in the direction of new technologies and new possibilities. It is evident that the percentage of mature aged people in this group is high, and here, one effective way to convince somebody to try something new, bringing mutual benefit both to a customer and a trader and ecology of the country in general, is through personal contact;
- 4 % of respondents have experienced a negative result in an attempt to pass on to a new mode of electricity consumption;
- A large group of respondents (19 %)are not aware of the new potentialities in the sphere of energy resource management and saving;
- 17 % are ready to try something new provided that they are convinced of the benefits from it;
- A relatively small percentage of respondents (9 %) are ready to take part in modelling their expenditures and energy consumption management through mobile game applications.

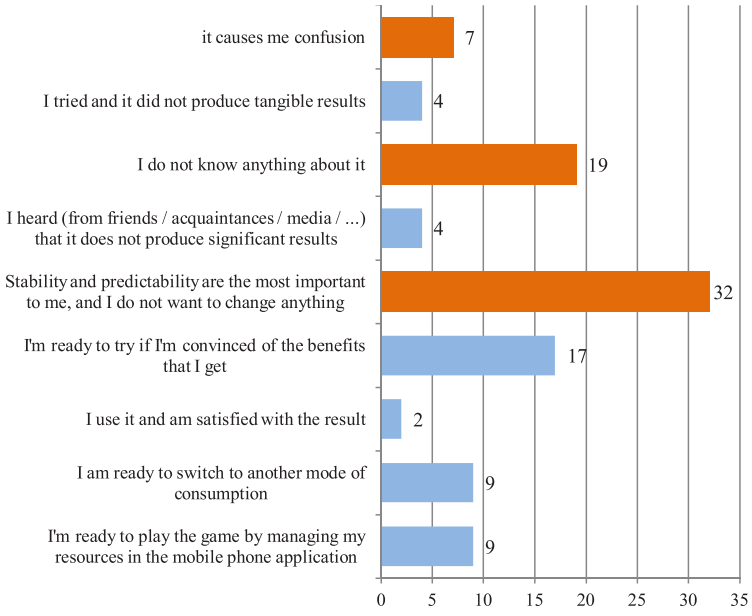

Fig. 8. "What do you think about choosing another electricity consumption mode for saving resources and money?"

There was quite a large group of respondents who knew nothing about new possibilities in the field of energy management and saving or wished to change noth-

ing or felt confused or uncertain (the group of replies marked in orange). Here, further research could be oriented towards finding the reasons for such unawareness and non-acceptance. One possible reason could be using insufficient information sources excluding widely used types such asTV, radio and the internet. If this is the case, new information dissemination channels should be searched for, say, in public transport, at the cash desk in a shop, as advertisement in mobile games etc.

5. CONCLUSIONS

Overall, survey findings show that awareness of the Latvian inhabitants of the processes related to formation of more smart or intelligent cities is not quite high. Many people prefer not to try new possibilities and technologies enabling one to be energy efficient in the field of resource consumption. Conservatism and unwillingness to lose the today's comfort level reached make them stick to frequently unprofitable consumption conditions from the economic point of view, but the lack of information does not further enlarge knowledge of the topic. Plenty of useful, up-to-date energy saving technologies and equipment could be available in the Latvian market, but the lack of interest and willingness to use them would reduce to zero all possible economic effects of such innovations.

Nevertheless, as the research shows, many people are willing to learn more and it is important to them to have and extend the overall picture of what is happening in the electric energy market so as to be able to actively participate in decision-making. Furthemore, in modern world, multidisciplinary studies are becoming increasingly requested that combine knowledge and competences from the spheres that aretraditionally considered different. Electric engineering and smart consumption of energy resources, on the one hand, and awareness of inhabitants and their active participaton in consumption management, on the other hand, if combined together, would further promote the most rapid and confident progress in a stable development of a smart city in general and smart management of the resources of every inhabitant of Latvia in particular. The issue of personal values and priorities of each consumer is one of the major issues in the successful strategy of city development, which contains possibilities and challenges to change habits and persuasions to more energy efficient, active and conscious ones.

ACKNOWLEDGEMENTS

The present publication has emanated from research supported by the ERA-NET-Lac grant under the ERANet-LAC 2nd Joint Call on Research and Innovation for Latin America, Caribbean and European Union Countries, Project ID: ELAC2015/T10-0643.

REFERENCES

1. European Smart Cities. (n.d.). Available at http://www.smart-cities.eu/download/smart_cities_final_report.pdf

2. Sustainable Development Strategy of Latvia until 2030. (n.d.). Available at https://www.pkc.gov.lv/sites/default/files/inline-files/Latvija_2030_7.pdf
3. Riga Smart City Sustainable Energy Action Plan for 2014–2020. (n.d.). Available at http://www.rea.riga.lv/files/RIGA_SMART_CITY_SEAP_2014-2020_EN.pdf
4. Schuitema, G., Ryan, L., & Aravena, C. (2017). The consumer's role in flexible energy systems. *IEEE Power & Energy Magazine*, *15*(1), 53–60. DOI: 10.1109/MPE.2016.2620658
5. Lattelecom. (2017). Informatīvs materiāls par elektroenerģijas tirgu Latvijā un tā jauno spēlētāju Lattelecom ar zīmolu tet. Available at https://www.likta.lv/LV/Presei/Lists/Biedru_relizes_pazinojumi/Attachments/139/tet_informativais%20materials.pdf
6. U.S. Department of Energy. (2014). Customer Participation in the Smart Grid –Lessons Learned. Available at https://www.energy.gov/sites/prod/files/2014/10/f18/SG-CustParticipation-Sept2014.pdf
7. Central Statistical Bureau of Latvia (n.d.). Available at https://www.csb.gov.lv/en
8. Jans, L.,Bouman, T., & Fielding, K. (2018). A part of the energy "in crowd". *IEEE Power & Energy Magazine, 16*(1), 35–41. *DOI:* 10.1109/MPE.2017.2759883.

IEVADS VIEDO PILSĒTU ENERGOEFEKTIVITĀTES PRINCIPOS: TEHNOLOĢIJAS UN APZINĀTĪBA, LATVIJAS PIEREDZE

A.Mutule, J.Teremranova

K o p s a v i l k u m s

Pilsētplānošana kļūst par mūsu gadsimta neatņemamu sastāvdaļu, un saskaņā ar dažādām prognozēm turpmākajās desmitgadēs 60 % - 80 % planētas iedzīvotāju pārcelsies uz pilsētām. Šis process lielā mērā ir objektīvs, jo tas veicina produktīvas aktivitātes palielināšanos daudzās jomās un vienlaikus palīdz atrisināt sabiedrības sociālās ekonomiskās problēmas. Nav šaubu, ka viens no vissvarīgākajiem virzieniem viedo pilsētu attīstībā ir sasistīts ar elektroenerģiju, jo īpaši ekonomisko un efektīvo enerģijas un siltuma ražošanas tehnoloģiju ieviešanā, pilsētas energoresursu un siltumapgādes drošībā, enerģijas taupīšanas tehnoloģijas un materiālu un iekārtu energoefektīvā lietošanā, nodrošinot ilgāku to ekspluatācijas laiku.

Enerģijas patēriņš ir cieši saistīts arī ar uzņēmējdarbības aktivitāti un iedzīvotāju dzīves līmeni. Lielāko uzmanību pievēršot pilsētu iedzīvotājiem un tā ieradumu maiņai, ir iespējams sasniegts daduz augstāku energoefektivitātes līmeni. Rakstā sniegts pārskats par pašreizējo situāciju Latvijas iedzīvotāju izpratnē mūsdienu enerģijas taupīšanas tehnoloģiju jomā. Autori iepazīstina ar plašu datu klāstu, kas iegūti pētījumā par iedzīvotāju attieksmi pret jaunām tehnoloģijām un gatavību sekot viedās pilsētas attīstības tendencēm.

Rakstā ir iekļauta analīze un ieteikumi energoefektivitātes uzlabošanai un energoefektīvu tehnoloģiju ieviešanai katrā mājsaimniecībā, lai radītu vislabvēlīgākos apstākļus ilgtermiņa plānu izstrādei viedo pilsētu attīstībai Latvijā.

27.11.2018

sciendo

LATVIAN JOURNAL OF PHYSICS
AND TECHNICAL SCIENCES
2018, N 6

INDEX OF PAPERS PUBLISHED IN 2018

PHYSICAL AND TECHNICAL ENERGY PROBLEMS

SOLID STATE PHYSICS

PHYSICS

sciendo

LATVIAN JOURNAL OF PHYSICS
AND TECHNICAL SCIENCES
2018, N 6

2018. GADĀ PUBLICĒTO RAKSTU RĀDĪTĀJS

ENERĢĒTIKAS FIZIKĀLĀS UN TEHNISKĀS PROBLĒMAS

CIETVIELU FIZIKA

FIZIKA

sciendo

LATVIAN JOURNAL OF PHYSICS
AND TECHNICAL SCIENCES
2018, N 6

УКАЗАТЕЛЬ СТАТЕЙ, ОПУБЛИКОВАННЫХ В 2018 ГОДУ

ФИЗИКО-ТЕХНИЧЕСКИЕ ПРОБЛЕМЫ ЭНЕРГЕТИКИ

ФИЗИКА ТВЕРДОГО ТЕЛА

ФИЗИКА

ПРИКЛАДНАЯ ФИЗИКА

ЭЛЕКТРОННАЯ СВЯЗЬ

МЕХАНИКА